Climate Dynamics
https://doi.org/10.1007/s00382-022-06249-6

Impact of air–sea coupling on the simulation of Indian summer monsoon using a high-resolution Regional Earth System Model over CORDEX-SA

Alok Kumar Mishra[1] · Pankaj Kumar[1] · Aditya Kumar Dubey[1] · Gaurav Tiwari[1] · Dmitri V. Sein[2,3]

Received: 11 January 2022 / Accepted: 7 March 2022

Abstract
A new high-resolution Regional Earth System Model, namely ROM, has been implemented over CORDEX-SA towards examining the impact of air–sea coupling on the Indian summer monsoon characteristics. ROM's simulated mean ISM rainfall and associated dynamical and thermodynamical processes, including the representation of northward and eastward propagating convention bands, are closer to observation than its standalone atmospheric model component (REMO), highlighting the advantage of air–sea coupling. However, the value addition of air–sea coupling varies spatially with more significant improvements over regions with large biases. Bay of Bengal and the eastern equatorial Indian Ocean are the most prominent region where the highest added value is observed with a significant reduction up to 50–500% precipitation bias. Most of the changes in precipitation over the ocean are associated with convective precipitation (CP) due to the suppression of convective activity caused by the negative feedback due to the inclusion of air–sea coupling. However, CP and large-scale precipitation (LP) improvements show east–west asymmetry over the Indian land region. The substantial LP bias reduction is noticed over the wet bias region of western central India due to its suppression, while enhanced CP over eastern central India contributed to the reduction of dry bias. An insignificant change is noticed over Tibetan Plateau, northern India, and Indo Gangetic plains. The weakening of moisture-laden low-level Somalia Jets causes the diminishing of moisture supply from the Arabian Sea (AS) towards Indian land regions resulting in suppressed precipitation, reducing wet bias, especially over western central India. The anomalous high kinetic energy over AS, wind shear, and tropospheric temperature gradient in REMO compared to observation is substantially reduced in the ROM, facilitating the favourable condition for suppressing moisture feeding and hence the wet bias over west-central India in ROM. The warmer midlatitude in ROM than REMO over eastern central India strengthens the convection, enhancing precipitation results in reducing the dry bias. Despite substantially improved ROM'performance, it still exhibits some systematic biases (wet/dry) partially associated with the persistent warm/cold SST bias and land–atmosphere interaction.

Keywords Indian summer monsoon · Air–sea coupling · RESM · ROM · CORDEX-SA

1 Introduction

The Indian summer monsoon rainfall (ISMR) is changing in the warming climate; however, the nature of the change is heterogeneous over the region like Indian subcontinents (Rajeevan et al. 2008; Pattanaik and Rajeevan 2010; Roxy et al. 2017). It is needless to mention the necessity of the accurate prediction of ISMR on a regional scale, which affects billions of people (Rajeevan et al. 2008). However, its prediction or projection has posed a great challenge, especially on the regional scale. Indian summer monsoon (ISM) is a coupled atmosphere–ocean phenomenon (Charney and Shukla 1981). Thus, the better representation of air–sea

✉ Pankaj Kumar
kumarp@iiserb.ac.in

[1] Department of Earth and Environmental Sciences, Indian Institute of Science Education and Research Bhopal, Bhopal 462066, India

[2] Alfred Wegener Institute for Polar and Marine Research, Bremerhaven, Germany

[3] Shirshov Institute of Oceanology, RAS, Moscow, Russia

Published online: 02 April 2022

coupling is crucial towards improving monsoonal characteristics. Numerous studies have reported the lack of air–sea coupling in the standalone atmosphere model is one of the fundamental sources of uncertainty highlighting the necessity of coupled models. In recent decades, significant efforts have been made to develop coupled models to improve the prediction or projection of ISMR and enhance the understanding of associated physical and dynamical processes. A good number of earth system models (ESMs) that participated in the coupled intercomparison project (CMIP5) is able to reproduce the large-scale features, however, inadmissible for projecting the ISMR and its extreme characteristics on the regional scale due to huge uncertainty (Sperber et al. 2013; Kumar et al. 2013). The spread in CMIP's models and huge uncertainty remains to persist from its phase 3 (CMIP3) (Meehl et al. 2007), intermediate phase 5 (CMIP5) (Taylor et al. 2012), and even in recent most advanced phase 6 (CMIP6) (Stockhause and Lautenschlager 2017) towards simulating the ISMR especially regional scale (e.g. homogeneous regions) (Meehl et al. 2007; Stroeve et al. 2012; Kitoh et al. 2013; Sperber et al. 2013; Saha et al. 2014; Sein et al. 2015; Parth Sarthi et al. 2015; Sabeerali et al. 2015; Kitoh 2017; Ashfaq et al. 2017; Aadhar and Mishra 2020). Despite the significant improvement (including physics and refinement of resolution), these models are still not suitable for projecting the regional monsoonal characteristics over India mainly due to its coarse resolution, which limits the resolving of the complex topography and its interaction with different components of the systems (Kripalani et al. 2003; Ashfaq et al. 2009; Saha et al. 2014; Sabeerali et al. 2015; Aadhar and Mishra 2020).

Regional models have an added value for realistically representing finer scale information and resolving the topography, physics, and dynamics (Giorgi 2019). Numerous studies have investigated the performance of regional climate models (RCMs) in simulating the ISM characteristics and reported substantial improvements in comparison to its parents GCMs or reanalysis (Dash et al. 2006; Saeed et al. 2009; Lucas-Picher et al. 2011; Jacob et al. 2012; Kumar et al. 2013, 2014; Mishra and Dwivedi 2019; Mishra et al. 2020a, b; Rai et al. 2020; Kumar 2021; Mishra et al. 2021a, b). Despite the substantial improvements, RCMs still have not gained the confidence of optimum level, probably due to the lack of regional air–sea interaction (Lucas-Picher et al. 2011). The regional coupled atmosphere–ocean model or regional earth system model (RESM) models are crucial to understanding strongly associated coupled features and their nonlinear complex interaction over the complex region like Indian subcontinents and, hence improving the prediction of ISMR. Nowadays, several RESMs have been developed for simulation over different CORDEX domains, including CORDEX-SA; however, it is still in its early stages (Xue et al. 2020). These RESMs have been employed in a wide range of applications over different regions of the globe (Ren and Qian 2005; Hagos and Cook 2009; Li and Zhou 2010; Zou and Zhou 2013, 2016; Klingaman and Woolnough 2014; Ratnam et al. 2015; Sein et al. 2015; Cha et al. 2016; Sitz et al. 2017; Zou 2020; Xue et al. 2020). However, very few attempts have been made to investigate the ISM characteristics on the regional scale using RESMs (Ratnam et al. 2009; Samala et al. 2013; Misra et al. 2017; Di Sante et al. 2019; Mishra et al. 2021a, b). For the first time, a high-resolution regional earth system model (RESM), namely ROM (Sein et al. 2015) (having a resolution higher than state-of-the-art global earth system models) employed over CORDEX-SA to investigate the impact of air–sea coupling on ISMR and associated dynamical and thermodynamical processes. This resolution is higher than earlier studies using any global ESM for climate change projections and advanced assessment studies. This model has been used over different parts of the globe and has proven good potential in simulating the fields over its standalone atmospheric model REMO (Sein et al. 2020; Zhu et al. 2020; Cabos et al. 2020). A rigorous evaluation of model skill is required to gain confidence in reliability. Moreover, numerous studies have investigated the climate model's skill in simulating the ISM characteristics (Dash et al. 2006; Kumar et al. 2006, 2013; Mishra et al. 2020b). However, most of the studies are restricted only to surface parameters which can help identify the bias in the fundamental characteristics but neglect the origin of uncertainty in these parameters. This study performed an in-depth evaluation of the ROM in reproducing the ISMR and associated surface characteristics and thermodynamical and dynamical process's vertical structure.

2 Components of the RESM and experimental design

In this study, a new high-resolution RESM, namely ROM, is implemented over CORDEX-SA towards improving the ISMR. ROM comprises a set of three models (i) limited-area REgional MOdel (REMO) (Jacob 2001) is atmospheric components (ii) Max-Planck Institute Model MPIOM (Marsland et al. 2003; Jungclaus et al. 2013) coupled with sea-ice and marine biogeochemistry model HAMOCC (Marsland et al. 2002) and (iii) Hydrological Discharge model HD (Hagemann and Dumenildumenil 1998) is hydrological components. All model components are coupled via the OASIS coupler (Valcke 2013) with a coupling frequency of 24 h for the HD model and a high coupling frequency of 3 h (coupled time step) for the atmosphere and ocean that ensures a realistic representation of the diurnal cycle. The high coupling frequency and the inclusion of tidal dynamics led to improve the representation of the regional high-frequency interaction

that was neglected in most of the global models. The atmosphere–ocean coupling is performed over the coordinated regional downscaling experiments (CORDEX) for South Asia (CORDEX-SA) (Fig. 1). The REMO exchanges heat flux, water flux, winds, and surface air pressure to MPIOM, whereas the MPIOM exchanges sea surface temperature (SST) to REMO. We briefly describe the individual components setup of the coupled model used in this study below.

2.1 Ocean components

The Max Planck Institute Ocean Model (MPIOM) (Jungclaus et al. 2013) is taken as the oceanic component of the coupled setup, which is coupled with the sea ice model (Hibler 1979) and biogeochemistry using a Hamburg ocean carbon cycle model (Marsland et al. 2002). The MPIOM is coupled with an integrated dynamic or thermodynamic with viscous-plastic rheology sea ice model. The biogeochemical

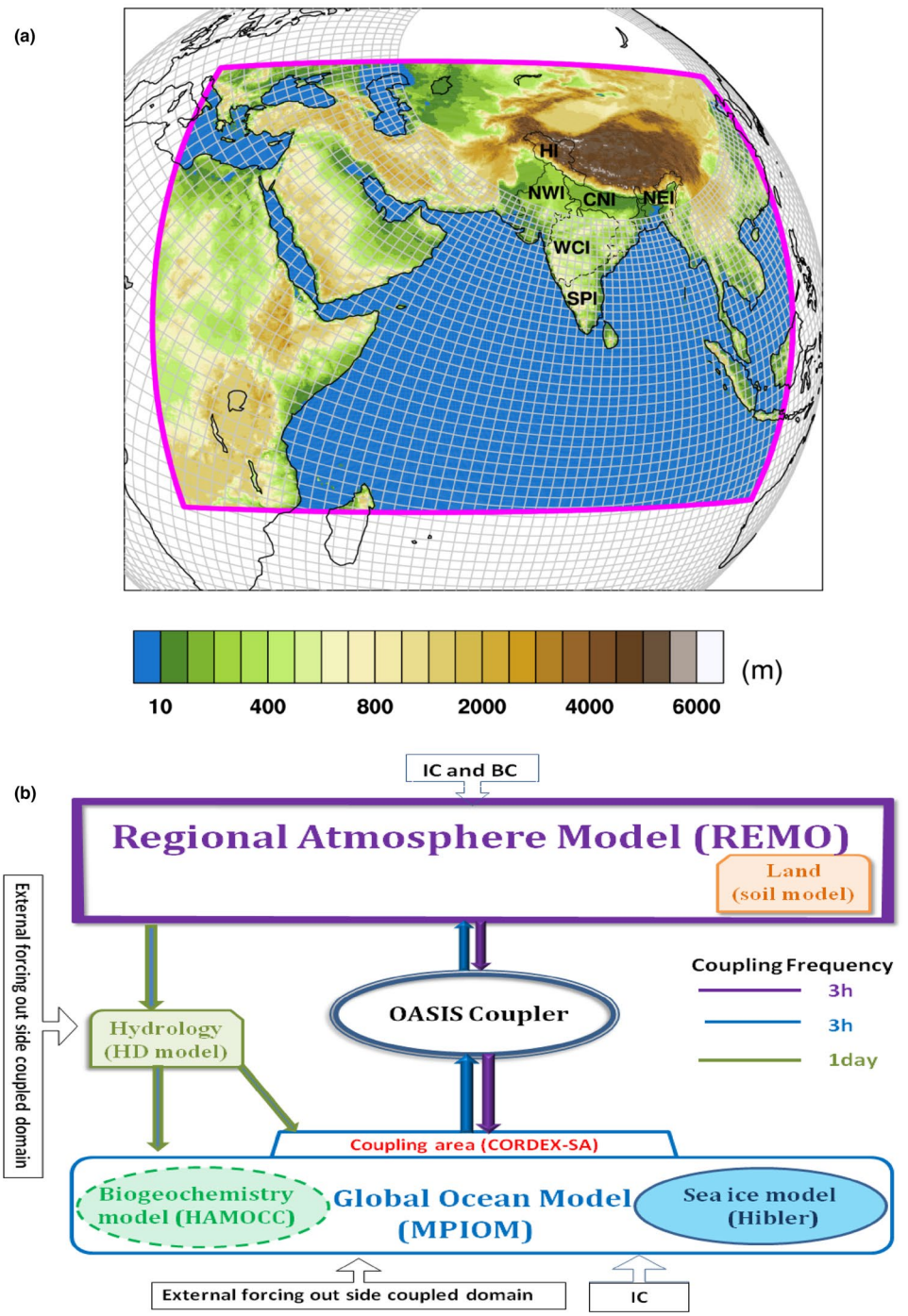

Fig. 1 Model topography (**a**). The six Indian homogeneous rainfall zones, namely HI, NWI, WCI, CNI, NEI, and SPI, are also shown. The pink box shows the region of air–sea coupling in ROM. The Systematic representation of the Regional Earth System Model (RESM) over the CORDEX-South-Asia region (**b**). Arrows represent the interaction among different components. The dotted block components are not active in this study

model uses a radiation scheme same as in the Ocean model, to compute photosynthesis and advection and mixing for tracers. The MPIOM is formulated with the hydrostatic approximation covering the global domain, which makes it different from the conventional regional earth system models that rely on information provided by the global ocean model at the lateral boundaries (LB), creating several issues (Sein et al. 2020). For example, (i) inconsistencies between the regional model solution and the LB data due to differences in resolution or physics of LB source (ii) uncertainty on the influence of coastal waves originating from outside the target region (beyond coupled domain consisting regional ocean model). The use of the global ocean model overcomes these complications, which brings significant advantages for climate change scenario simulations. For instance, it allows for the investigation of possible long-term changes in some oceanic extreme events that are generally not possible in regional ocean models due to monthly mean data as a lateral boundary condition.

An orthogonal curvilinear grid facility in MPIOM allows the varying horizontal resolution (higher resolution over the target region and region having more complexities). This study employed a maximum resolution of 5 km (eddy-permitting) over the coastal region, ~ 10 to ~ 20 km in the Indian Ocean, and a minimum resolution of about 100 km in the southern seas. We use 40 unevenly spaced vertical z-levels and incorporate ocean tides' influence. The model is also equipped with tidal forcing, derived from the full ephemerides lunisolar tidal potential (Thomas et al. 2001). The MPIOM uses bottom boundary layer slope convection (Marsland et al. 2003), Gent and McWilliams's eddy-induced mixing parameterization, and an isopycnal diffusion scheme (Griffies 1998). As MPIOM is integrated globally, no lateral boundary is required; however, it is initialized with Polar Science Center Hydrographic Climatology (PHC) (Steele et al. 2001). The external atmospheric forcing and upper oceanic boundary conditions outside the coupled domain are prescribed with atmospheric fields obtained from ECMWF ERA-Interim (EIN) reanalysis (Dee et al. 2011). The same reanalysis is also used as boundary conditions for standalone REMO. The 100-years of model simulation are discarded as spinup, and 38 years (1980–2017) of simulated fields are stored for analysis.

2.2 Atmospheric components

REMO is adopted as atmospheric components, which employed the physical parameterizations of the global climate model ECHAM versions 4 and 5 (Roeckner et al. 2003) and Europa-Model of the German Weather Service based dynamical core. It employed the Arakawa-C-grid and leap-frog scheme with time filtering by Asselin (1972) for spatial and temporal discretization. A semi-implicit correction is employed to allow longer time steps. The horizontal resolution of 0.22° (~ 25 km) in the rotated grid and 27 vertical levels following the hybrid sigma pressure coordinate is taken. The rotated grid avoids the disproportion of grids closer to the poles and takes care of the numerical singularity due to the convergence of meridians at the geographical North Pole allows us to avoid the largely different extensions of the grid cells close to the poles. We employed the implicit scheme for Vertical advection and turbulent to avoid numerical instabilities (Jacob and Podzun 1997). The fractional land surface scheme is adopted for the fractional land-surface scheme of Rechid et al. (2009) is utilized for land surface processes. The Tiedtke cumulus convection parameterization scheme of Tiedtke (1989) for the production of convective precipitation in the model. Additionally, a statistical cloud cover scheme of Tompkins (2002) is used to deal with cloud processes.

We adopted the common configuration and model domain (CORDEX-SA) for standalone and coupled simulation. We employed the six hourly varying ECMWF ERA-Interim (Dee et al. 2011) fields for lateral boundary conditions that are relaxed in the outer eight rows of the model area (relaxation zone or buffer zone) following (Davies 1976). The prognostic variables adjusted towards large-scale forcing in this buffer zone by exponential damping in this zone towards the inner model domain. This buffer is excluded from the analysis. The fractional land surface scheme is adopted for the land-surface process (Rechid et al. 2009). The SST obtained from ECMWF ERA-Interim is for carrying out the standalone REMO simulation (i.e. without oceanic model coupling). The model results are stored for 38 years from 1 January 1980 to 31 December 2017 after removing the initial transients (50 years of spinup).

2.3 Hydrological components

We employed a Hydrological Discharge model (HD) (Hagemann and Dümenil 1998) that is integrated globally with 0.50° horizontal resolution. It provides the continental runoff to the ocean model and delivers freshwater discharge at the exact river mouth. The REMO model computes the fields at 0.22° horizontal resolution. Over coupled domain, the ocean and atmosphere exchange the fields every three hours.

2.4 Observational data

For evaluating the simulated precipitation, we have used daily high-resolution (0.25° × 0.25°) India Meteorological Department (IMD) gridded daily mean rainfall for the Indian land region. It is obtained from daily rainfall records from 6955 rain-gauge stations, which is till now the highest number of stations used for any kind of gridded data available over India (Shashikanth et al. 2014). Additionally, the high spatial (10 km) and temporal (3 hourly) resolution

Multi-Source Weighted Ensemble Precipitation (MSWEP) data covering land and ocean is also used to demonstrate the performance in simulating the precipitation northward and eastward propagation. This data is the merged product of satellite (infrared and microwave), rain gauge, and reanalysis (Beck et al. 2019). The monthly convective and large-scale precipitation is obtained from Tropical Rainfall Measuring Mission (TRMM) Microwave Imager Precipitation Profile L3 1 version 7 (*V7)* (*TRMM_3A12*). This data is available for 1997-12-01 to 2015-04-01 at $0.5° \times 0.5°$ horizontal resolution that can be obtained from https://disc.gsfc.nasa.gov/datacollection/TRMM_3A12_7.html. For the winds, air temperature, and specific humidity, the latest released ERA5 reanalysis data set (Hersbach et al. 2020) at a ~ 30 km resolution grid is utilized. The sea surface temperature data is obtained from the Hadley Centre Global Sea Ice and Sea Surface Temperature (HadISST). HadISST uses reduced space optimal interpolation applied to SSTs from the Marine Data Bank (mainly ship tracks) and ICOADS through 1981 and a blend of in-situ and adjusted satellite-derived SSTs for 1982-onwards.

2.5 Method of estimating the northward and eastward propagation

In this study, the northward and eastward propagating convecting bands have been computed following the methodology of Sabeerali et al. (2013). Firstly 20–100 days bandpass filtered has been applied for precipitation to extract the intraseasonal mode. Then, the filtered precipitation is regressed for both propagation modes at each grid against a reference time series. The averaged filtered precipitation over the region 12° N–22° N and 70° E–90° E is taken as reference time series for the northward propagation while averaged precipitation over 10° S–5° N and 75° E–100° E is used as reference time series for eastward propagation. The lag-longitude map averaged over 5° S–5° N and a lag-latitude map averaged over 70° E–95° E is used to represent the eastward propagation and northward propagation. This comparison is made for the 1998–2014 availability of data period of TRMM.

3 Results

The comparative skill assessment of the ROM and its standalone model REMO is necessary for gaining confidence in the individual model set up, and further quantifying the impact of air–sea interaction over the region. Therefore, this study rigorously compared ROM and REMO model's skills in simulating the Indian summer monsoon rainfall and associated dynamical and thermodynamic processes.

3.1 Performance and air–sea coupling impact assessment for precipitation

Figure 2 shows the JJAS mean precipitation during the study period for the IMD observation (a) ROM (b) and REMO (c). The figure depicts that both models reasonably reproduce the spatial distribution of mean seasonal JJAS precipitation. It distinguishes the regions of low precipitation (North-west India, Northern India, and southern India) and high precipitation (the Western Ghats, Northeast India (NEI), and Central India). However, REMO shows the shift in the high precipitation region over north-central India towards the southwest and produces relatively large amounts of precipitation compared to observation and ROM. The precipitation bias map (Fig. 2d, e) for ROM and REMO suggests that REMO exhibits a dipole like the structure of bias having dry bias over the northeast central Indian region and wet bias over southwest central India. A substantial reduction of these biases is noticed in ROM, suggesting a considerable role of air–sea coupling toward improving the seasonal mean precipitation. The biases remain within one standard deviation of JJAS rainfall in ROM except for a few places. Moreover, the value addition of air–sea coupling varies spatially, with more significant improvements over regions having a large wet (dry) bias.

The sources of moisture for different subregions of India and different months are found to vary (Pathak et al. 2017). Therefore it is worthwhile to demonstrate the temporal evaluation of bias to isolate the hidden error caused by a different source. Figure 3 depicts the evidence of regional variability in bias, which varies within the monsoon season. It can be seen from the figure that REMO sustained huge wet bias throughout the entire monsoon season; however, magnitude is found to be varying spatiotemporally. The least wet bias is observed during the initial phase of the monsoon (June) over south-central Indian, which was found to intensify June onwards with a southeastward propagation and widening the area of wet bias and attains the maximum value during the withdrawal period (September). The magnitude and area of wet biases are reduced and northward shifted during all months in the ROM simulation. The maximum dry bias (4-5 mm/day even more) is noticed during the peak phase of monsoon over east-central India. This dry bias central is substantially lower (0–1 mm/day), indicating ~ 60–80% improvement during July. The other months also show improvement but less than during the peak phase. Interestingly during the first half of the monsoon phase (June–July), ROM shows dry bias over east-central India and wet bias in the latter half phase, compensating in computing the mean JJAS bias. This highlights the necessity of temporal evaluation of model bias. Although there is a coherent signal of improved precipitation in ROM throughout the monsoon season, the figure does also suggest some

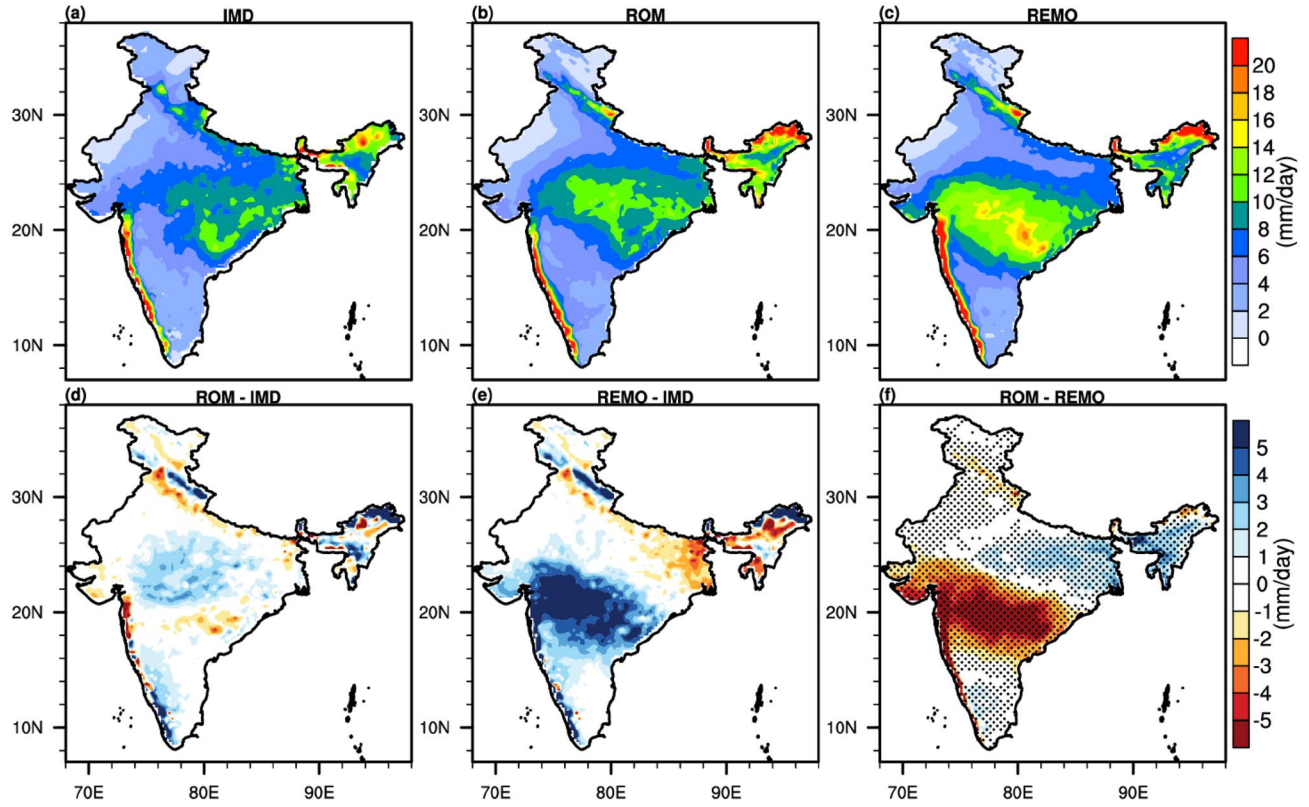

Fig. 2 Seasonal (JJAS) mean rainfall (mm/day) from **a** IMD **b** ROM and **c** REMO and biases (model-IMD) **d** ROM—IMD and **e** REMO—IMD and impact of air–sea coupling **f** ROM-REMO. The black dots represent grid points having a 95% confidence level

areas over northern India, particularly during June and July, where ROM's performance is found to degrade.

We also computed the bias with another observation (TRMM) covering land and ocean (Fig. 4) to demonstrate the ROM's performance over ocean. From the figure, it can be noticed that the bias with respect to TRMM is more or less similar to bias with respect to IMD for the Indian land region. REMO shows huge overestimation over the Bay of Bengal (BoB), eastern equatorial Indian ocean, and some part of southeast Arabian Sea throughout the season, which is substantially reduced in the coupled experiments (ROM), and even wet bias is replaced by dry bias (lesser magnitude than that in REMO). The replacement of wet bias with dry bias may be associated with cold SST bias over BoB. The systematic overestimation of precipitation in standalone simulations is due to the absence of coupled feedbacks (atmospheric response to the underlying SST). The favorable local prescribed SST conditions continuously favor the deep convection to remain active over the BoB and, hence, precipitation resulting in huge wet bias over the region. In contrast to this, the active fine-scale two-way air–sea feedback over this region in ROM tends to cool the SST, which results in suppressing the convection and hence precipitation. This result aligns with the studies (Ratnam et al. 2009; Hirons et al. 2018; Di Sante et al. 2019). Despite substantial improvement over most of the region, the equatorial region of the southern hemisphere shows the intensification of dry bias due to air–sea coupling.

Further, the impact of air–sea coupling is investigated for the temporal evolution of precipitation over the Indian homogeneous region of rainfall (IHRR) (Parthasarathy 1995; Mishra et al. 2020b) for daily climatology of 38 years (1980–2017) by computing various statistical metrics (for example, root mean square error (RMSE) and standard deviation (Std. Dev.) and percentage improvements (added value). The added value is computed following Eq. (1), and the results are summarized in Table 1.

$$Added\ value = \frac{RMSE_{REMO} - RMSE_{ROM}}{RMSE_{REMO}} \times 100. \quad (1)$$

The table depicts the reduction of RMSE compared to REMO, confirming the advantage of air–sea coupling. Overall ROM shows substantial improvement relative to REMO over the entire Indian land region; however, the magnitude of RMSE reduction and percentage improvement varies with region. The highest improvement is noticed over WCI (56.75%), whereas the lowest is over CNI (8.99%).

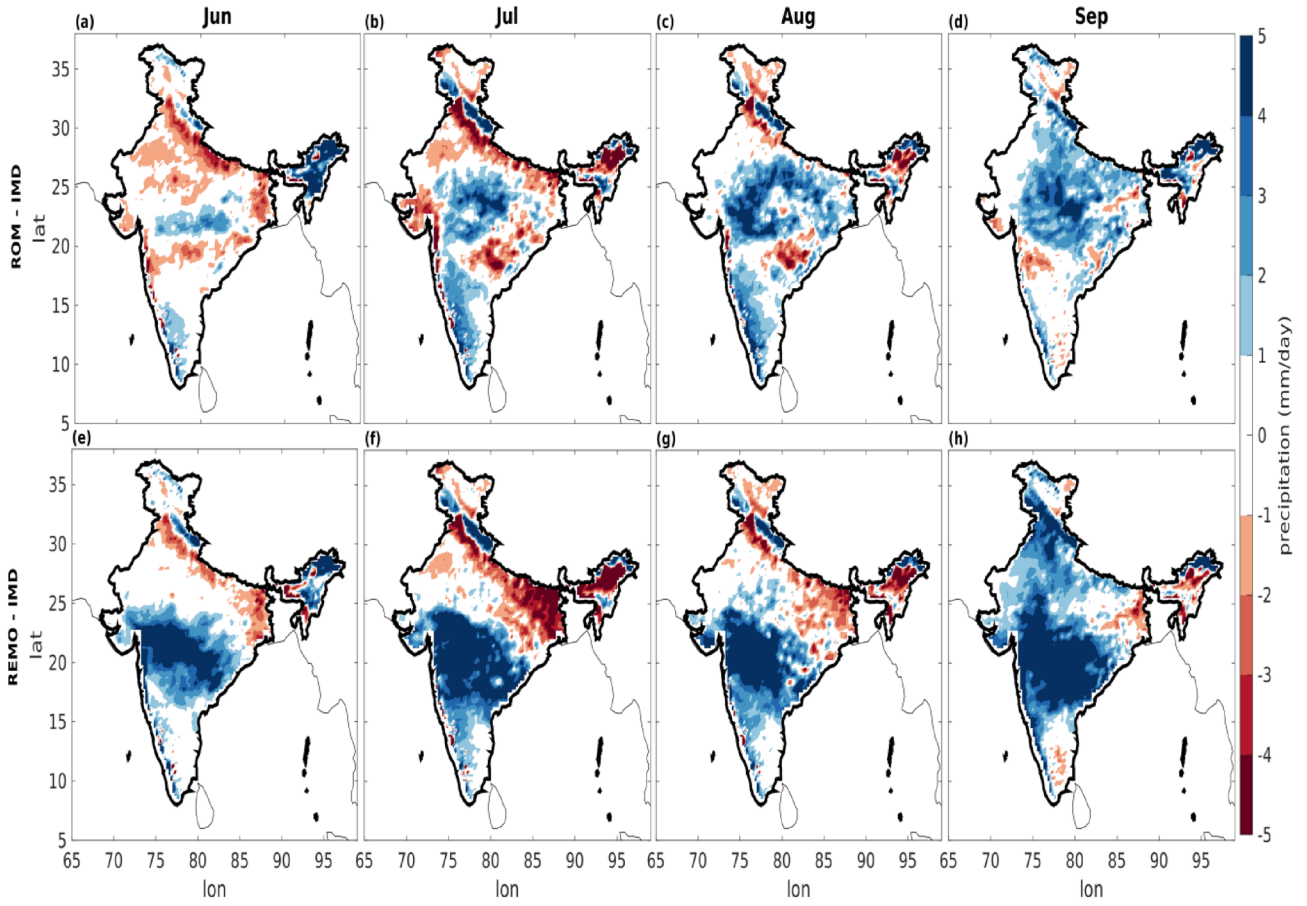

Fig. 3 Monthly precipitation bias (mm/day) ROM—IMD (upper panel) and REMO—IMD (lower panel) during June–July–August–September for 1980–2017

The correct partitioning of total precipitation between the convective precipitation (CP) and large-scale precipitation (LP) relies on the reliability of model physics responsible for producing the individual type of precipitation. For example, the convective parameterization (subgrid-scale moisture) scheme derived the CP(LP), which is also known as the unresolved (resolve) scale of precipitation.. It is vital to examine the impact of air–sea coupling on the individual precipitation type and identify the weakness concerning physics. Figure 5 represents the bias map of precipitation, CP, and LP. The biases are computed by subtracting the individual types of JJAS mean observed precipitation during 1998–2014 of TRMM from corresponding simulated values of ROM and REMO. Here, we have taken only 1998–2014 due to the availability of TRMM data. The figure represents the contrasting nature of bias in precipitation over the Bay of Bengal (BoB) and Arabian Sea (AS). For example, the wet (dry) bias is noticed over the southern (northern) BoB and north (south) AS in REMO. Moreover, the magnitude of the bias is comparatively lesser (~ − 1 to 1 mm/day) over AS than the BoB (> − 8 to 8 mm/day). The wet/dry bias is also noticed over southwest/northeast central India. The equatorial Indian Ocean (EIO) shows wet bias, which varies from ~ 6 mm/day and is even greater than 8 mm/day in some places. These wet and dry biases over AS and BoB are consistent with previous studies (Kumar et al. 2013, 2020; Ashfaq et al. 2017; Di Sante et al. 2019; Mishra and Dwivedi 2019) attributed to the lack of ocean–atmosphere coupling (Ratnam et al. 2009; Hirons et al. 2018). These uncertainties are found to be reduced in our ROM simulation. The convection in the coupled models leads to the formation of clouds and precipitation, consequently cooling the SSTs and suppressing the convection and hence precipitation. As coupled models use the feedback from the atmosphere and ocean, warm SST on the first day leads to strong convection that feeds back to cool the SST for the next day. This next day's cool SST then forced the atmospheric model. In contrast to this, warmer SST in RCMs continuously supports convection (due to the absence of precipitation feedback on SST), and hence precipitation results in the release of latent heat in the atmosphere and produces the wet bias. As a standalone atmospheric model is being forced using observed

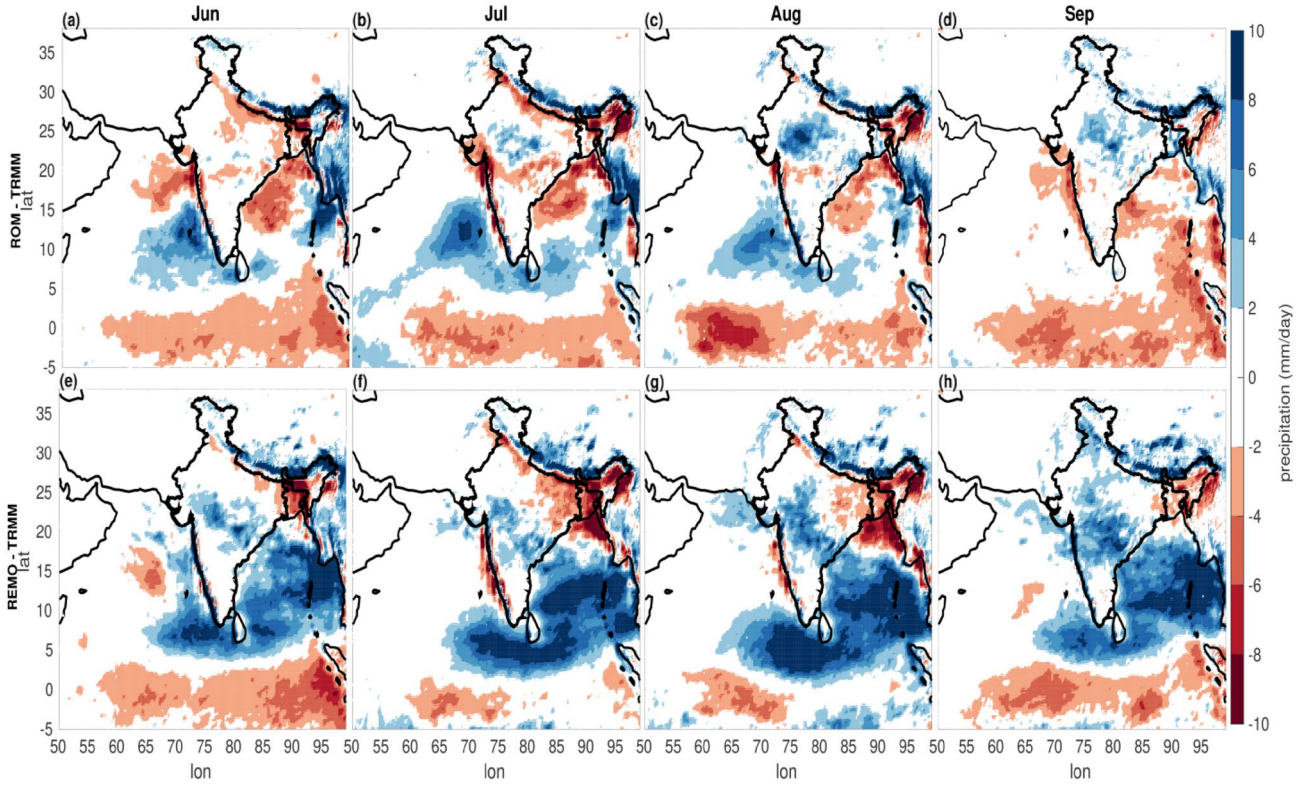

Fig. 4 Monthly precipitation bias (mm/day) ROM—IMD (upper panel) and REMO—IMD (lower panel) during June–July–August–September for 1998–2014

Table 1 Performance evaluation of ROM and REMO with statistical analysis over the six Indian homogeneous rainfall zones

Zone	ROM/REMO RMSE	Improvements or added value (%)
CNI	1.72/1.89	8.99
NWI	1.31/2.78	52.88
NEI	2.49/2.89	13.84
WCI	1.57/3.63	56.75
SPI	1.92/3.25	40.92
HI	1.53/2.10	27.14

These values are computed at 99% significance level

SST, warm SST one day might lead to strong convection that does not feedback to cool the SST for the next day.

The improvement of precipitation in ROM is a combined impact of improvement in CP and LP. However, regions of improvement in the individual types of precipitation are heterogeneous. For example, precipitation improvement is primarily associated with CP over the ocean, while both LP and CP contribute to TP's improvements over lands. Moreover, the improvement due to CP is dominant over eastern central India, while over western central India, the gain is mainly associated with LP. On the contrary, some regions where insignificant improvements are seen for TP, CP, and LP are also noticed. For example, similar dry (wet) bias is found to be persisted in REMO and ROM over the Tibetan Plateau, northern India, and Indo Gangetic plains suggesting an insignificant impact of air–sea coupling over these regions.

3.2 The mechanism associated with precipitation difference caused by air–sea coupling and precipitation bias

Although this study aims to investigate the impact of air–sea coupling on ISMR and major focus has been directed to the atmospheric component of the complex climate system; however, a strong relationship with the strength of the Indian monsoon and SST (Levine and Turner 2012; Srivastava et al. 2018; Mishra et al. 2020a) highlighted the necessity of demonstration of the reliability of SST simulation that could help determine the source of bias. Figure 6 shows the JJAS mean SST from ROM and corresponding observation along with their bias. The figure depicts a good resemblance to observation in representing the spatial distribution of SST. ROM clearly distinguishes the regions of low and high SST, however, it shows a systematic discrepancy in magnitude. A robust, warm bias (~ 1–2 °C) is noticed along with the Somalia-Oman upwelling region and cold bias (< 1 °C) over

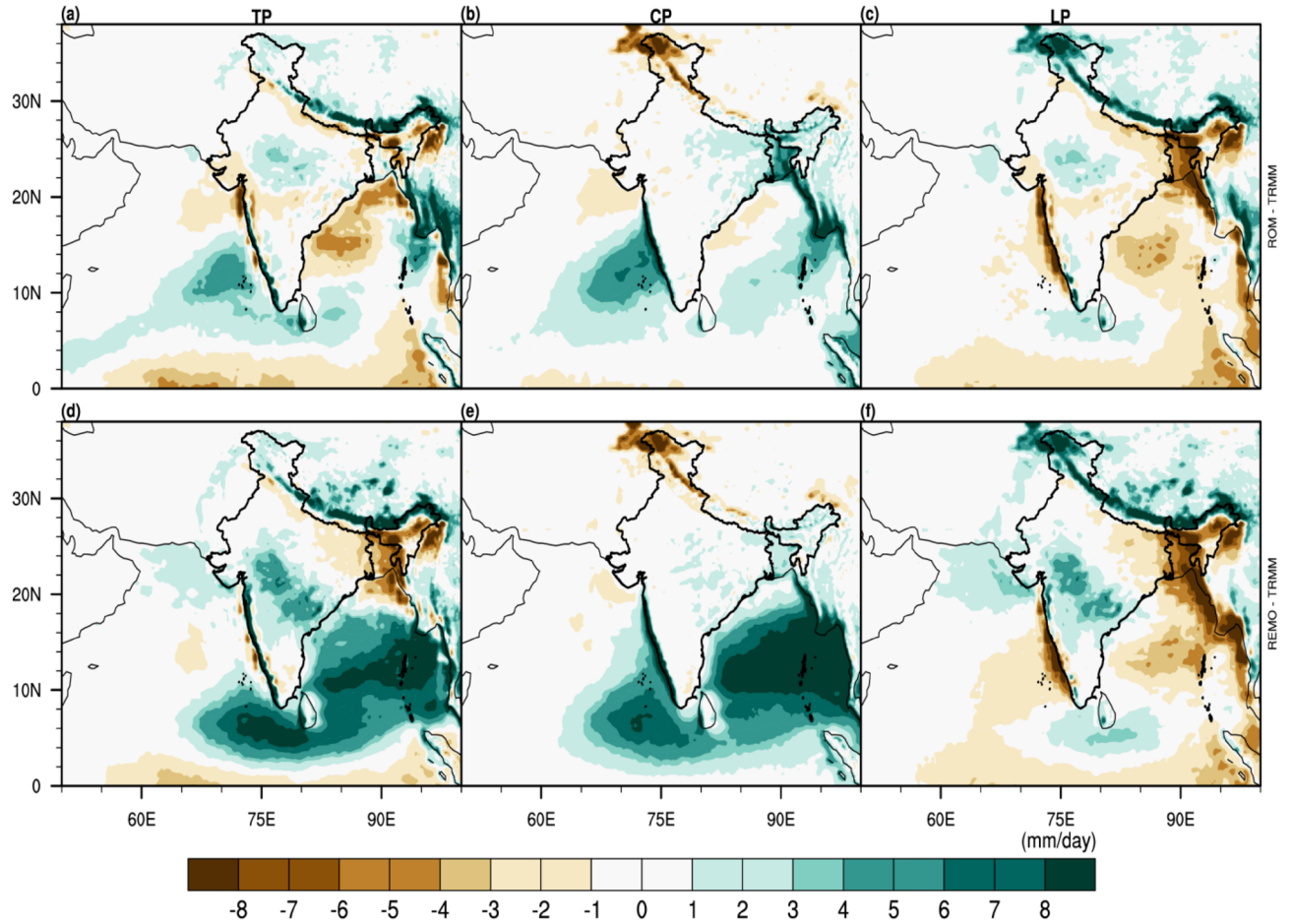

Fig. 5 Seasonal (JJAS) mean rainfall biases (mm/day) (model-TRMM) **a**–**c** for ROM: **a** for total precipitation, **b** for convective precipitation, **c** for large scale precipitation. **d**–**f** are similar to **a**–**c** but for REMO

BoB. The cold SST bias is the long-standing problem from the several generations coupled model having dry bias over India (Nagura et al. 2013, 2018; Sayantani et al. 2016; Fathrio et al. 2017). In general, the SST biases are lesser than the earlier reported studies using CMIP5/6 and regional ocean model over most of the northern Indian ocean, although there is a higher warm bias over the western Arabian Sea. This unrealistic warming over the western AS may be associated with reduced upwelling and weaker mixed layer depth caused by weaker wind (figure not shown). This anomalous warming further weakens the zonal SST gradient over the AS and hence southwesterly winds, which should substantially diminish the moisture supply towards India (Roxy et al. 2017).

Additionally, the cold bias over BoB suppresses the convection, and hence convective precipitation (as seen in Fig. 5) results in dry bias over the same region. To confirm the relationship between SST and precipitation bias, we computed the correlation of SST bias (interannual time series averaged over the Arabian Sea and Bay of Bengal) and precipitation of every grid over the Indian land region (Fig. S3). The Arabian Sea and BoB SST bias substantially correlated with precipitation bias over the Indian land region with spatially varying magnitude and nature. Barring a few patches, the wet (dry) bias areas in ROM are consistent with negative (positive) correlations with BoB SST bias. In comparison to BoB bias correlation, AS bias correlation shows more heterogeneity.

Apart from this, we also investigate the monthly variability of SST bias to examine its connection with the monthly virility of precipitation bias. Figure 7 depicts a similar bias structure throughout the monsoon season with some regional and magnitude differences. In general, the warm SST bias along the path of low-level Jet sustained in all months, but it is minimum in Jun and starts intensifying Jun onward. The maximum value is noticed in the peak phase then again decreased in September. Interestingly the cold bias over northern AS in Jun tends to become positive June onward and replaced by warm bias in August, leading to northward shifting of the south-westerly wind and hence moisture

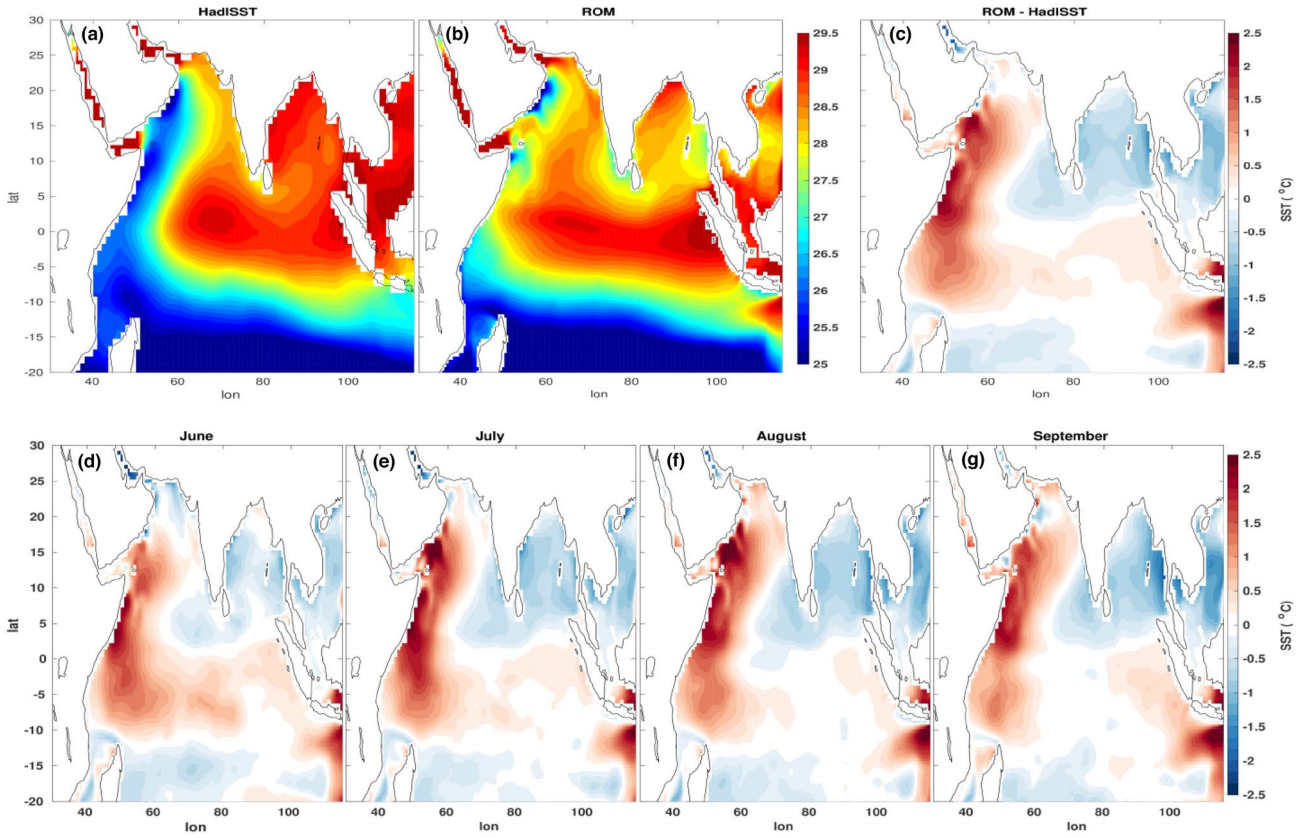

Fig. 6 Seasonal (JJAS) mean SST (°C) from **a** HadlSST **b** ROM and **c** JJAS mean biases (ROM-HadlSST) and monthly bias for **d** June **e** July **f** August **g** September

supply over the low precipitation region of northwest India (NWI). This partially supports the wet bias over NWI. The BoB wet also shows intensification Jun onward and maximum in September, which is consistent with the wet bias over BoB (Fig. 4).

The eastward and northward propagating convective bands from the Indian Ocean (IO) significantly regulate the intraseasonal variability and amount of precipitation the ISV of ISMR (Sperber and Annamalai 2008; Sabeerali et al. 2013; Di Sante et al. 2019). However, limited efforts have been made to understand the role of air–sea coupling on these propagating bands (Di Sante et al. 2019). Therefore, it is worthwhile to demonstrate the ROM's capability and influence of air–sea coupling in representing the northward and eastward propagation. It can be seen from Fig. 7 that REMO shows weaker or insignificant northward propagation over the ocean and also north of 25 N while ROM exhibits some propagation. ROM shows substantial improvement in the representation of northward convective bands, particularly over 10 S–7 N. Additionally, slight improvement is also noticed overland region north of 10 N, however, both models show an unrealistic representation of the convection band south of the 10 S. The minimal and no improvement due to air–sea coupling is partially related to persistent SST bias and partially due to the dominant role of atmospheric internal dynamics of the coupled system. Some earlier studies have also highlighted the role of the atmospheric internal dynamics as underlying mechanisms for this propagation (Jiang et al. 2004, 2011; Abhik et al. 2013). From Fig. 8, it can be noticed that REMO exhibit weaker eastward propagation of convection anomalies from EIO, particularly over 70 E–100 E, and even propagation in the opposite direction over west of 55 E and east of 100 E. ROM shows significant improvement in the representation of eastward propagating bands over the same region. This improvement partially supports the realistic simulation of mean precipitation.

The low and upper-level circulation pattern over the Indian subcontinent and adjoining oceans are one of the essential dynamical drivers of ISM. The strength and timing of low-level jets (LLJ) over the Indian subcontinent strongly control the IMSR by modulating the moisture coming from AS and get influenced by the air–sea interaction. Therefore it is vital to examine the model's potential and impact of air–sea coupling in representing the circulation. Comparison of simulated wind at 850 hPa from both models for all months of JJAS during the study period with corresponding

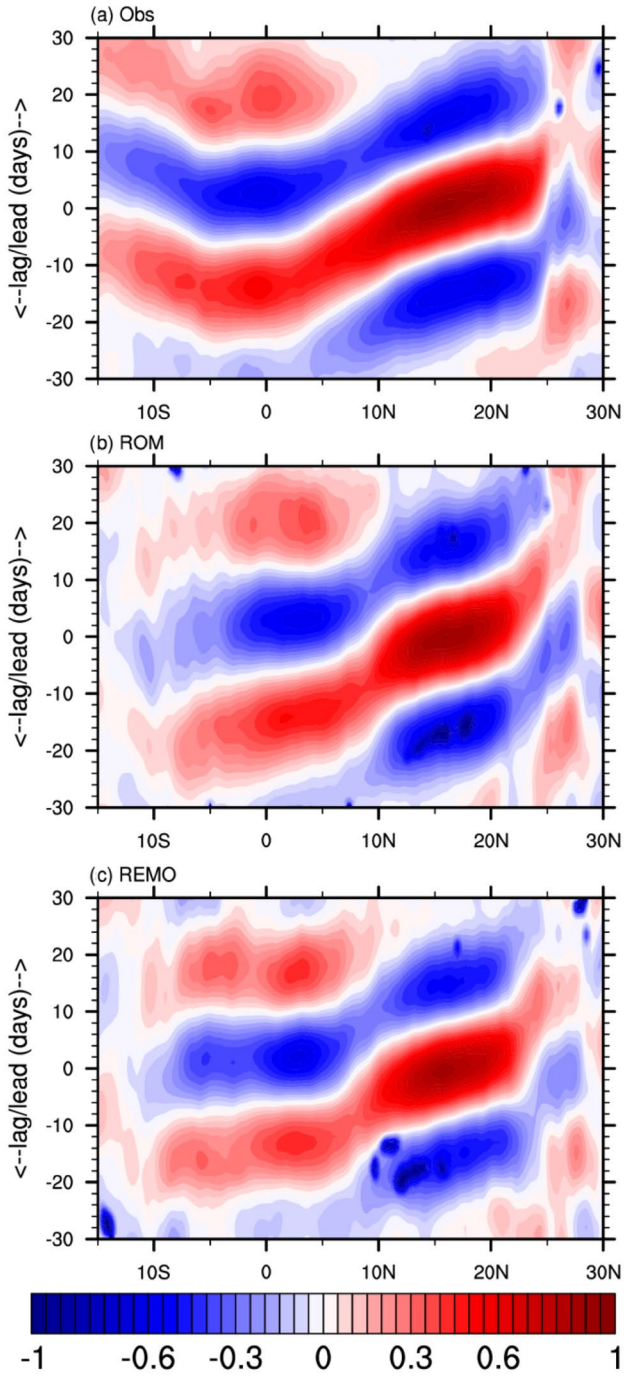

Fig. 7 Northward propagation: Lag-latitudes regressed anomalies of 20–100 days bandpass filtered precipitation (shaded; mm/day) band with reference time series averaged for a box over the Tropical Indian Ocean (10° S–5° N to 75° E–100° E)

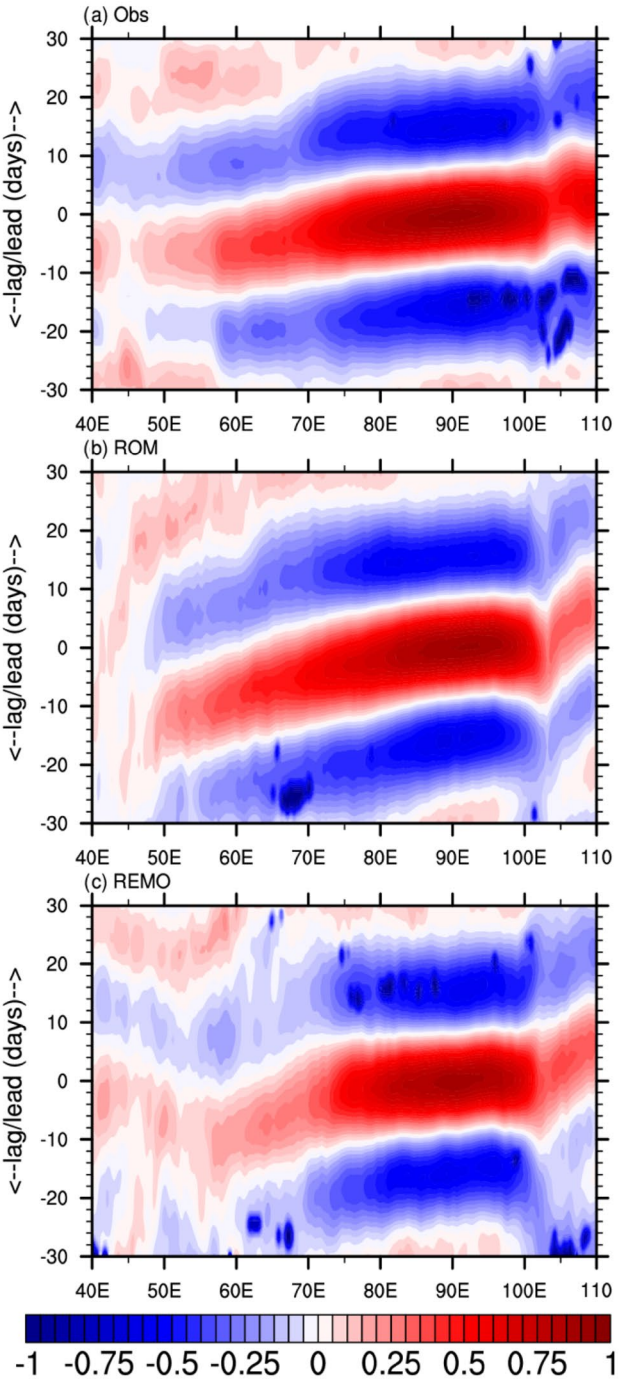

Fig. 8 Eastward propagation: Lag-longitudes regressed anomalies of 20–100 days bandpass filtered precipitation (mm/day) for 5° S and 5° N averaged band with reference time series averaged for a box over the Tropical Indian Ocean (10° S–5° N to 75° E–100° E)

observation (Fig. S1) indicates substantial month-to-month variability in observation for circulation, particularly LLJ, with moderate strength (15–20 m/s) and confined over the narrow region during June and intensified and widen with propagating northeastward in subsequent months and attain its maximum value (20–25 m/s) in the peak phase of monsoon month July. A slight decrease in strength is noticed after July, with a minimum value during September. Both models bear a close resemblance to observation in representing spatio-temporal circulation patterns; however, some

systematic discrepancy is seen in magnitude. In general, both models underestimate speed over the location of LLJ and overestimate over BoB and India; however, ROM shows weaker LLJ than REMO, which is consistent with lower precipitation over India in ROM. This weaker LLJ in ROM is possibly due to the warm SST bias over AS, reducing land-sea thermal contrast and pressure difference. As a result, ROM shows better skill in terms of strength of speed over India throughout the monsoon season. Similarly, we examine the model's potential for upper-level wind (Fig. S2). It can be seen from the figure that the models show good skill in simulating the large-scale feature of upper-level wind (e.i. sub-tropical jets; STJ and tropical easterly jets; TEJ and Tibetan high anticyclonic circulation), with some systematic difference in magnitude. The magnitude of STJ (TEJ) is higher (lower) in both models, with a slight improvement in ROM. Apart from this, some places are also seen where REMO is more close to observation.

For a more quantitative investigation of the air–sea coupling impact, we compute the difference of LLJ obtained from ROM and REMO (Fig. 9a–d). ROM shows a weaker LLJ than REMO throughout the monsoon season with a varying magnitude difference in all months over the IO, particularly over the core location of the LLJ, which diminishes the supply of moisture from AS towards Indian land (Kumar et al. 2006; Parth Sarthi et al. 2015; Roxy et al. 2017; Di Sante et al. 2019; Mishra et al. 2020a). The maximum difference for LLJ is noticed during the onset and withdrawal months. As a result, a wet bias in precipitation over southern and west-central India is reduced. On the other hand, a stronger wind speed over eastern central India in ROM than REMO increases the local moisture by increasing the evapotranspiration and produces more precipitation, reducing the dry bias over the same region. For upper-level wind, A anticyclonic flow (ACF) with the center over southern India. The divergent wind from AS converges over north-central India that becomes the upper branch of ACF. This upper-level convergent flow towards India, leading to subsiding motion transferring heat and momentum that eventually helps to suppress the ascending motion, leads to weakening the low-level cross-equatorial flow. It can be seen that the STJ is stronger and moves equatorward towards the Indian subcontinent from west of northwest India, particularly during withdrawal in ROM. In addition, stronger TEJ (3–5 m/s) also favor the stronger monsoon over central India.

The strength of moisture transport (either atmospheric or oceanic) regulates the precipitation during the summer monsoon. It is reported in the study by Pathak et al. (2017) that the contribution of oceanic (atmospheric) is larger during the first 2 months (later 2 months). The investigation of monthly variability of vertically integrated moisture flux (VIMF) might be helpful to provide a clue for a reason behind the bias of precipitation and association of change precipitation change due to air–sea coupling on moisture source impact of ISMR. Figure 10 represents the monthly climatology VIMF during monsoon season for models and observation, which is computed over 1000–300 hPa, following (Konwar et al. 2012) using Eq. (2)

$$\mathrm{VIMF} = \frac{1}{g}\int_{\mathrm{surface}}^{300\mathrm{hPa}} qV(u,v)dp, \tag{2}$$

where q is specific humidity, u and v are zonal and meridional components of wind, p represents the pressure, and g is the acceleration due to gravity.

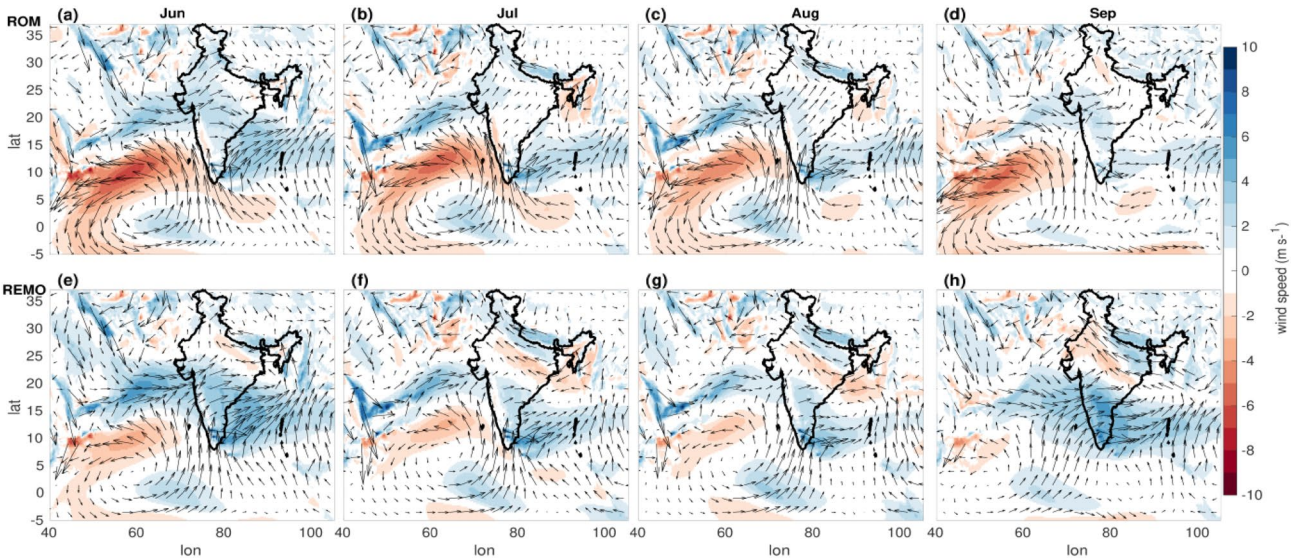

Fig. 9 Difference of monthly mean wind obtained from ROM and REMO (ROM—REMO) for 850 hPa (**a**–**d**) and 200 hPa (**e**–**h**). The positive values indicate a higher value in ROM and vice-versa

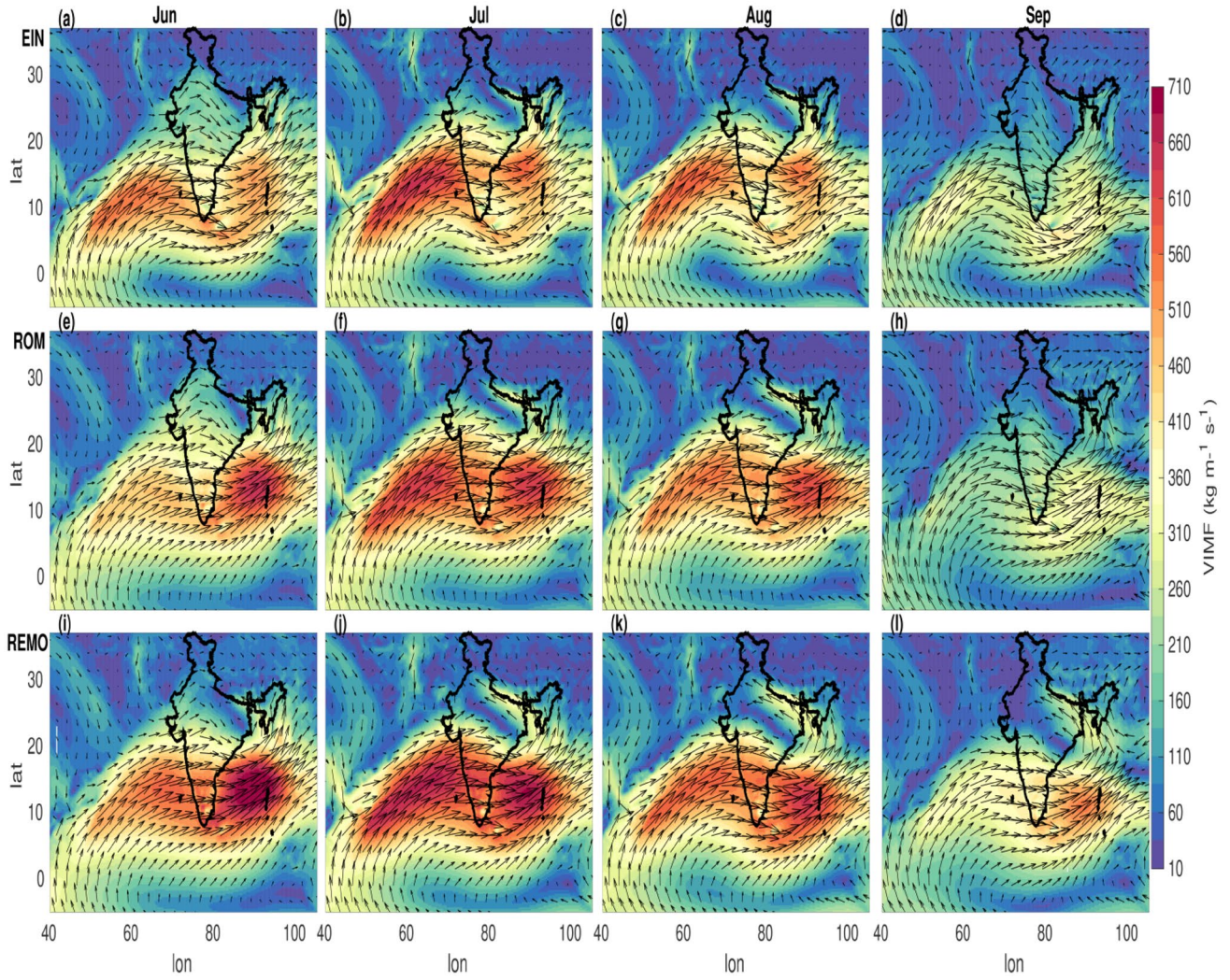

Fig. 10 Monthly averaged vertically integrated moisture (shaded represents the magnitude and vector represents direction) during the study period for EIN (**a**–**d**), ROM (**e**–**h**), and for REMO (**i**–**l**)

The figure reveals strong spatiotemporal variability of VIMF in EIN. The higher value is noticed over AS along the path of LLJ and BoB that also shows the month-to-month variability with the highest value during the peak month of monsoon (July). In addition, over northwest India, maximum values are noticed during June, decreasing in subsequent months of monsoon. These patterns are well represented by both models, with slight differences in magnitude compared to observation. In general, ROM is closer to observation than REMO.

To make results more prospective, quantitively, we computed the difference of VIMF obtained from model and observation (Fig. 11). REMO shows a substantial overestimation of VIMF over BoB, southern India, northern AS, and eastern central India while slight underestimation over central India. The inclusion of air–sea coupling in ROM reduces these overestimations substantially, which is consistent with the reduction of wet bias over BoB. The reduction of wet bias over the BoB in the ROM enhances the moisture supply from the BoB to the Indian land region, particularly over CI, leading to slight overestimation of VIMF over CI facilitating favorable conditions for precipitation, leading to reduction of dry bias. The magnitude of overestimation over CI in ROM is lesser than underestimation in ROM, indicating the better performance of ROM over this region. Despite the higher VIMF in REMO than ROM over east-central India, the divergent flow of transport and unfavorable conditions (weaker instability) for precipitation reduce precipitation. In contrast, enhanced wet bias over the AS is consistent with suppressed wet bias over western central India. The excess utilization of available local moisture over the same area (AS) is caused by the warm SST bias, weakened pressure gradient, and weaker wind, contributing to increasing the precipitation over AS and hence wet bias.

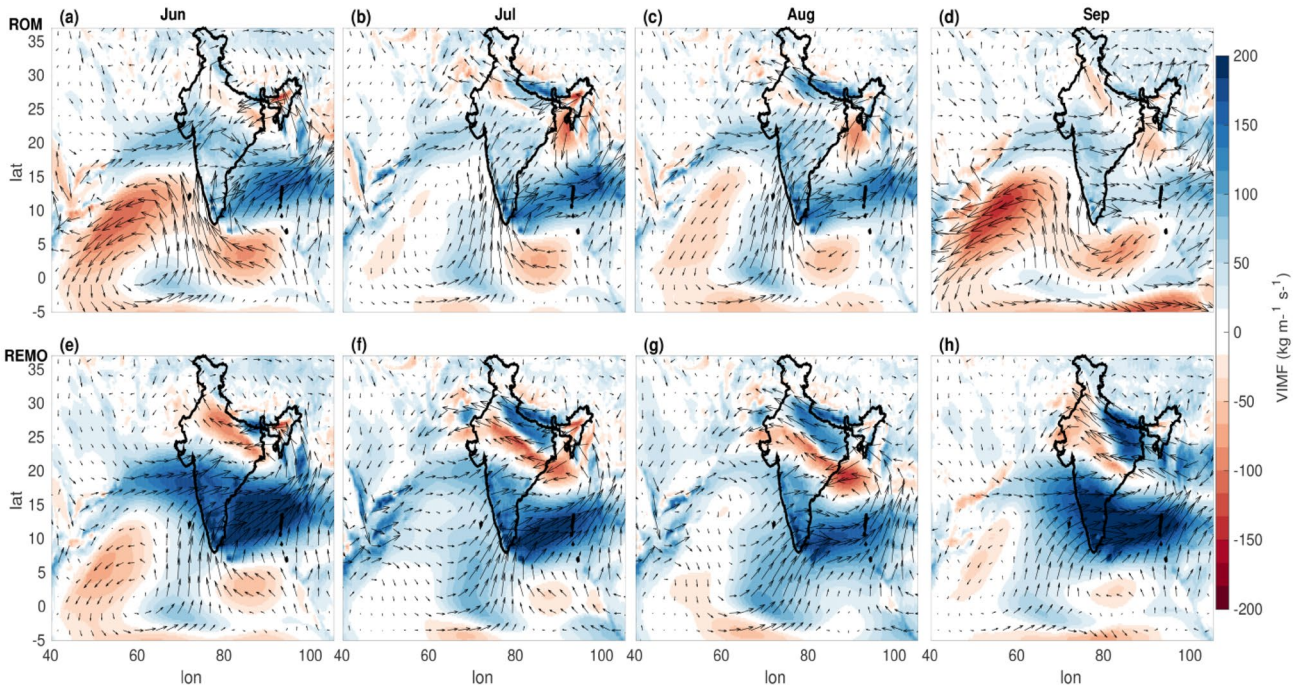

Fig. 11 Difference of monthly climatology of VIMF from model and observation (model-EIN) for ROM (**a**–**d**) and REMO (**e**–**h**)

It is worth diagnosing the large-scale dynamics and thermodynamics as a response of air–sea coupling contributing to the source of systematic differences in the precipitation in the ROM and REMO. Tropospheric temperature gradient (TTG) is an important thermodynamic index that tightly regulates the ISM's onset, withdrawal, and strength by regulating the large-scale circulation by modulating the north–south thermal contrast. In this study, TTG is computed following the method described in the study of (Goswami and Xavier 2005a). From the TTG map (Fig. 12), it can be noticed that for large parts of the year, the models (ROM and REMO) bear a close resemblance to ERA for temporal evolution between TTG and representing the reversal of the TTG sign. Both models seem very close together and equally biased compared to ERA except for onset and withdrawal phases. ERA data shows a positive gradient from the 1st June, climatological onset date, and changes to negative on 6th October, indicating the monsoon's withdrawal. Both model's results showed a slightly early reversal of negative to positive signs in the last week of May and a late reversal of positive to negative in the 2nd week of October, hence showing an early onset and delayed withdrawal (Table 2). However, ROM's simulated withdrawal and length of the rainfall season (LRS) are relatively closer to reanalysis than REMO's simulated values. We observed comparatively more considerable difference in the TTG curves during the onset and withdrawal phase than peak monsoon month (July–August), suggesting the more significant impact of air–sea coupling during the onset and withdrawal phase in modulating the thermodynamical monsoon index. Models showed a warmer TTG, especially from April to June; however, ROM's simulated warm bias is slightly less than REMO. This might be contributing to the wet biases respective model simulations as warmer (colder) TTG in pre-monsoon months have a substantial contribution in producing enhanced/suppressed precipitation over India (Singh and Chattopadhyay 1998; Kumar and Dimri 2020). The area under the TTG curve from the onset and withdrawal period is closely related to the monsoon's strength (Goswami and Xavier 2005b; Mishra et al. 2020b). The figure shows that the ROM showed slightly less area and became closer to observation, consistent with the corresponding reduction in precipitation.

Webster and Yang (WY) index (Webster and Yang 1992) based on the easterly wind shear is one of the important indexes that control the poleward propagation of the convection band and strength of the monsoon (Jiang et al. 2004). It also regulates the generation of the barotropic vorticity to the north of convection, leading to the northward shift of both the moisture convergence in the planetary boundary layer and the negative geopotential height in the lower troposphere and thus the northward propagation of the convection. WY is computed as the difference of lower and upper-level wind U_{850}–U_{200}, where U_{850} and U_{200} are the zonal wind at 850 hPa, and 200 hPa averaged over the region 40°–106° E; 0°–20° N. Figure 12 depicts the good skill of models in simulating the temporal evolution of the dynamical WY

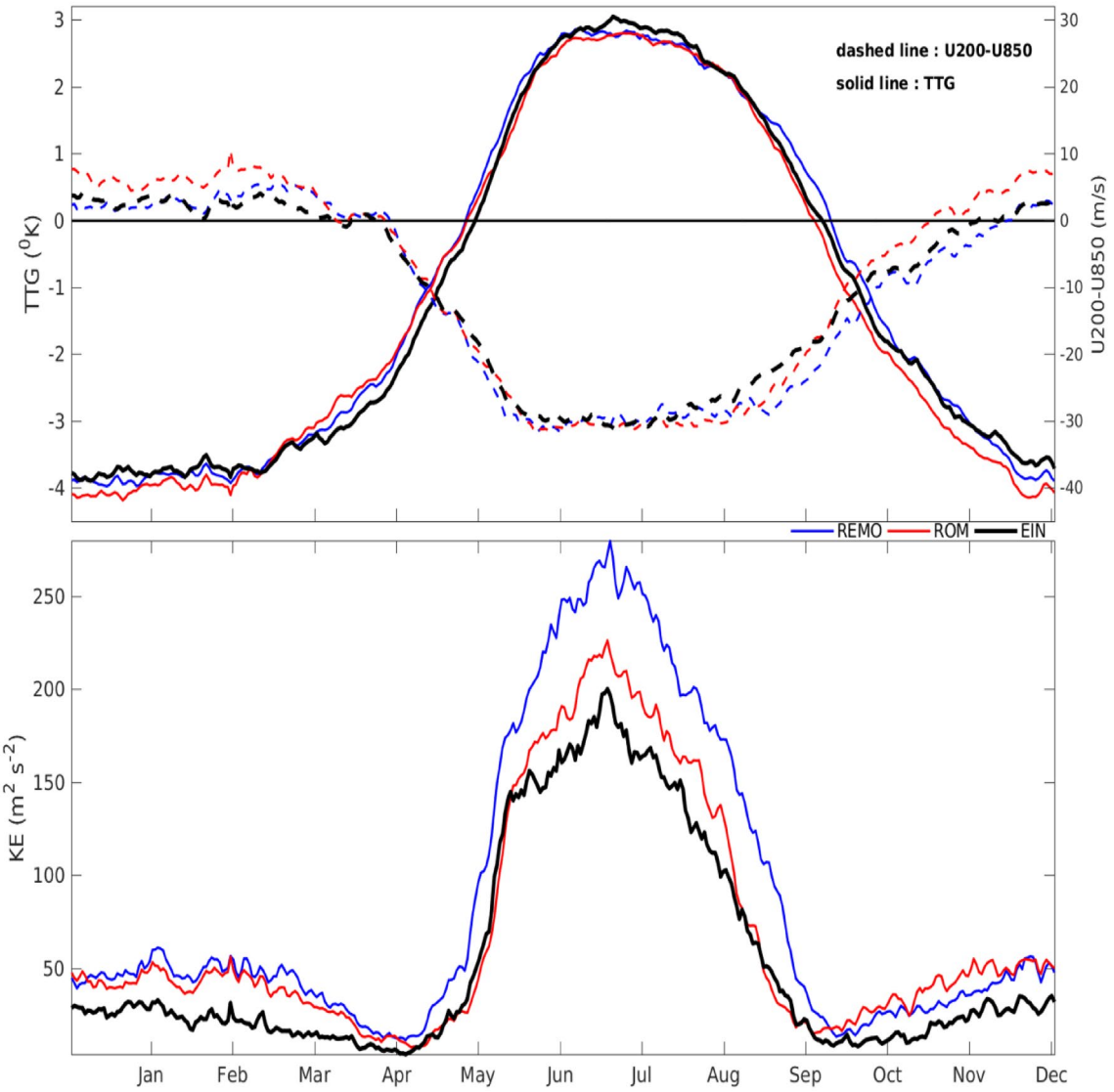

Fig. 12 Upper panel, mean meridional tropospheric temperature gradient (TTG; solid line) and Lower Panel, mean vertical shear of zonal winds (U200-U850; dashed line) averaged over the domain (50° E–95° E, 0–15° N). The daily climatology of kinetic energy (KE in $m^2\ s^{-2}$) at 850 hPa averaged over the domain (50° E–65° E, 5° N–15° N) is also shown; (lower panel)

Table 2 Climatological onset, withdrawal, and length of the summer monsoon season during 1980–2017

	Onset	Withdrawal	Length of the season (LRS)
EIN	1st June	6th October	129 days
ROM	29 May	7th October	130 days
REMO	29 May	13th October	136 days

index. Both models represent the similar evolution of the WY but differ slightly in the dates where the sign changes from positive to negative. The more considerable strength in the uncoupled model than the coupled model is one of the possible reasons for larger precipitation in REMO. Moreover, the more significant differences in ROM and REMO during the initial and withdrawal phase than peak monsoon phase again underline the fact that there is a comparatively more significant role of air–sea coupling during onset and withdrawal than peak monsoon phase. The spatial variation in the impact of air–sea coupling on the strength of the zonal wind's vertical shear is also investigated. Figure 13 shows the mean shear for models and observation. The figure depicts that ROM's simulated spatial distribution of shear is more or less similar to REMO but differs slightly in the shear strength. The ROM's simulated shear value is closer to observation than REMO, suggesting the advantage of air–sea coupling. It is noted that more considerable

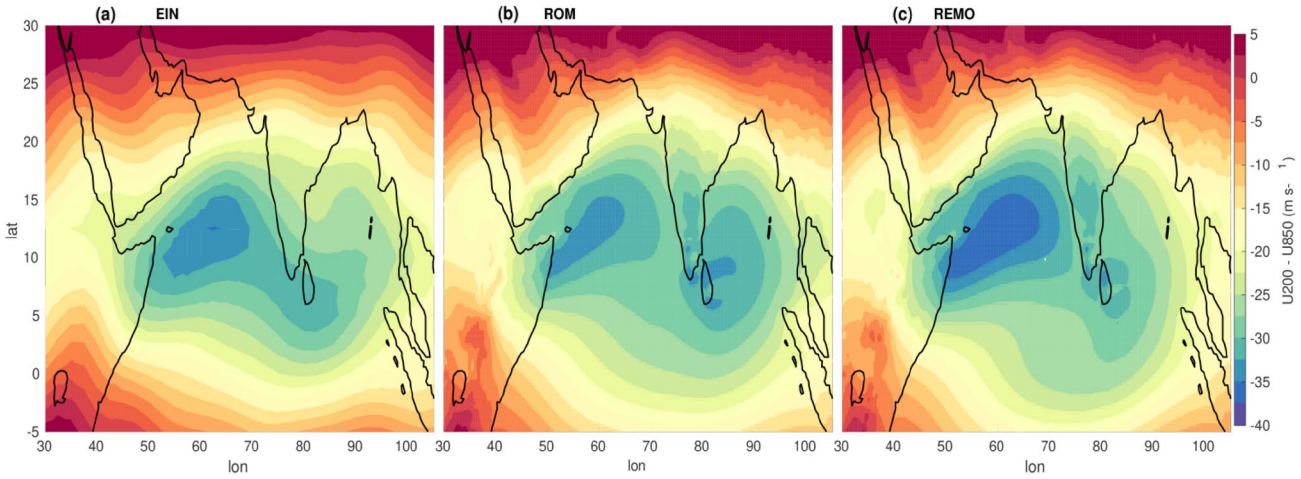

Fig. 13 Spatial distribution of mean vertical shear of zonal winds (U200–U850) from 1980 to 2017 **a** EIN **b** ROM and **c** REMO

value addition over AS. ROM shows lesser (greater) easterly shear over AS (BoB), resulting in the weakening (strengthening) of baroclinic instability. The considerably suppressed (strengthened) shear over AS (BoB) in ROM is consistent with the corresponding reduction (magnification) in precipitation over the western (eastern) part of CI.

The kinetic energy (KE) at 850 hPa over AS (50° E–65° E, 5° N–15° N) is one of the crucial dynamical parameters which have been used as a proxy for determining the onset date and strength of ISMR in earlier studies (Krishnamurti 1985; Goswami and Xavier 2005a; Mishra et al. 2020b). KE over AS also controls ISM's strength by modulating the moisture supply from AS to the Indian land region. Figure 12 depicts a rapid increase from June onwards, becomes maximum between July and August, and then starts to decrease rapidly, becoming minimum again in October. Both models well capture the seasonal variation of KE. However, ROM simulated KE evolution is closer to observation. It is also observed that the uncoupled model REMO produces a comparatively higher KE than the coupled version. The maximum KE obtained from REMO, ROM, and observation is 200, 226, and 279 m^2/s^2, respectively. This also shows a substantial advantage of air–sea coupling. The reduction in the KE in ROM is consistent with suppressed precipitation over India and hence wet bias.

To get more insight, the effort is made to examine the impact of air–sea coupling on the relationship of the different dynamical and thermodynamical indexes (e.g. WY, KE, TTG) with precipitation over India. Figure 14 represents the correlation between indexes and precipitation over India. It is observed that the TTG and KE show a positive correlation over central India and a negative correlation over northern and southern India. In contrast to this, WY shows a negative correlation over central India and a positive correlation over northern and southern India. Both ROM and REMO correctly reproduce these observed correlations and follow a similar correlation pattern of indexes with precipitation. This suggests that air–sea coupling has limited impact in modulating these indexes' relationship with precipitation over India. Despite substantial improvement in the ISMR and associated dynamical processes, ROM still shows some systematic dry/wet bias over eastern/western central India. Other factors may contribute to this systemic bias rather than the regional air–sea interaction and need to investigate the source of persistent bias further.

The vertical temperature structure has a coherent impact on precipitation strength (Raju et al., 2015). Therefore, it is crucial to address the impact of air–sea interaction on the vertical structure of the temperature and its association with wet and dry bias. We investigated the relative performance of ROM and REMO in simulating the vertical structure of temperature anomaly associated with the monsoon precipitation over the WCI/CNI roughly regions having wet/dry bias in REMO. Figure 15 represents the time height cross-section of temperature anomaly over the WCI and CNI region during the JJAS season. The figure depicts the contrast vertical structure of temperature anomaly before and after monsoon establishment. During the initial phase of the monsoon (June), warm (cold) temperature anomalies are noted in the lower (middle to upper) troposphere. In contrast, the reverse is happening after the monsoon establishment over Indian subcontinents. For example, the cold (warm) temperature anomalies are noted in the lower (middle to upper) troposphere from July onwards. Both simulations show a similar evolution of temperature anomaly over WCI and CNI with some intermittent variations in the anomalies' magnitude. Comparatively warmer midlatitude (700–400 hPa) in ROM than REMO noticed over CNI and vice-versa over WCI. The middle troposphere warming over CNI leads to the upper air divergence favouring the updraft and convection, enhancing

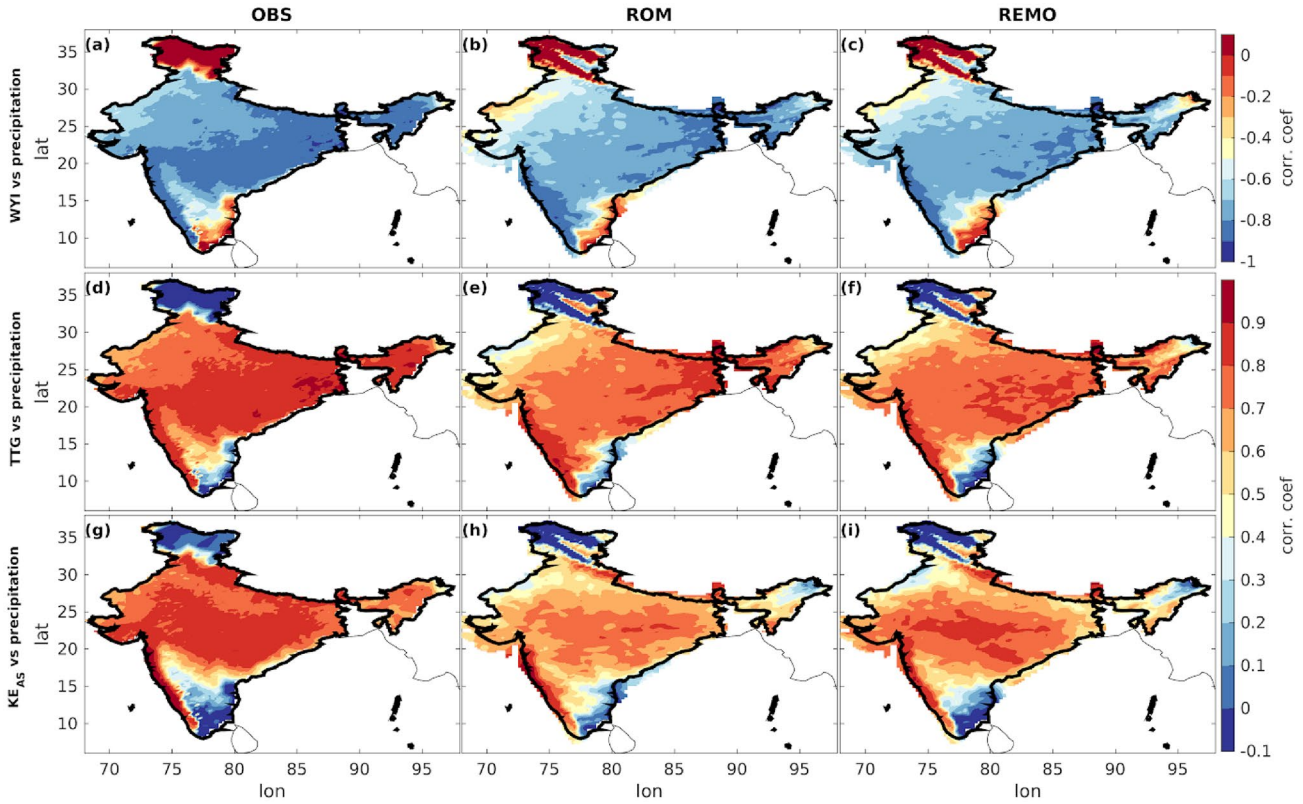

Fig. 14 Correlation coefficient of WYI, TTG, and KE with precipitation over India. For observation, IMD precipitation and Index are computed with EIN

precipitation over the same region (Raju et al. 2015; Mishra and Dwivedi 2019) and helping in reducing the dry bias. Moreover, the precipitation over WCI is affected by the dual nature of the mechanism, mid-tropospheric heating, and weakening of LLJ due to air–sea coupling. The warmer mid-tropospheric anomaly enhances the precipitation due to favorable conditions for the updraft and moist convective systems (Raju et al. 2015), however, this enhanced precipitation is largely compensated by the reduced precipitation due to suppressed moisture supply from AS due to the weakening of the LLJ, resulting in a net reduction in the precipitation due to air–sea coupling. A detailed study of the exact mechanism responsible for the persistent wet bias over WCI remains beyond the scope of this paper.

4 Conclusions

This study investigated the advantage of air–sea coupling using a high-resolution regional earth system model over the CORDEX-SA. The performance of the coupled ROM model and its standalone atmospheric model component (REMO) are accessed in simulating the mean Indian Summer Monsoon Rainfall (ISMR) and associated dynamical and thermodynamical processes. ROM's simulated ISMR and associated dynamical and thermodynamical processes bear a close resemblance to observation than REMO. The substantial reduction of biases in ROM compared to REMO highlights the benefit of air–sea coupling; however, considerable spatiotemporal variability of added value is noticed. The least wet bias is observed in ROM during the initial phase of the monsoon (June) over south-central India, which propagated southeastward and expanded in terms of its area in subsequent months of monsoon and attains the maximum value during the withdrawal period (September). ROM significantly reduces the maximum dry bias ~ 3–4 mm/day over east-central India during July, indicating ~ 60–80% improvement. Despite substantial improvements in ROM, some systematic bias with temporal variability in its nature is still noticed. For, example during the first half of the monsoon phase (June–July), ROM shows dry bias over east-central India and wet bias in the latter half phase, compensating in computing the mean JJAS bias. This highlights the necessity of temporal evaluation of model bias. In general, a coherent signal of improved precipitation in ROM is noticed throughout the monsoon season.

In general, the regions with stronger/weaker bias are consistent with greater/smaller value addition regions. The

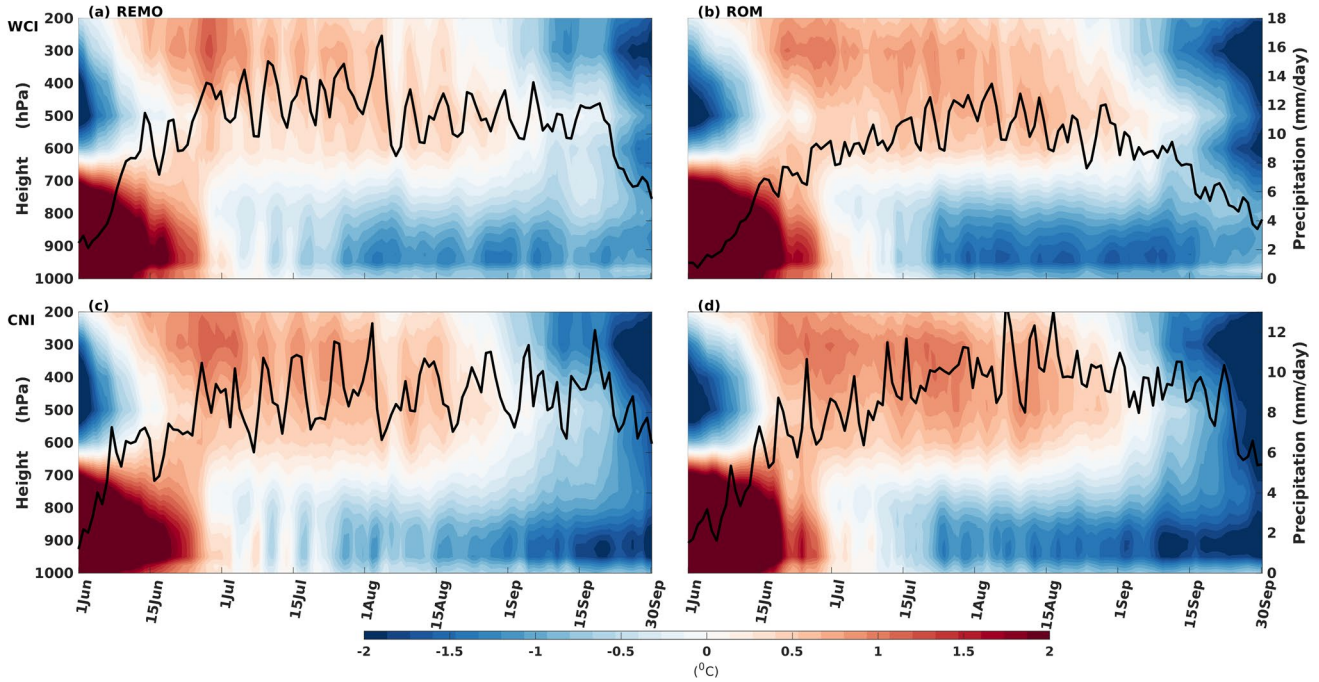

Fig. 15 The vertical structure of temperature anomaly over the WCI region for REMO (**a**) and ROM (**b**) during the JJAS season. Similarly, (**c**) and (**d**) for the CNI region

improvement over the ocean is considerably more significant than that of over Indian land regions. The BoB and EIO are the most prominent regions affected by air–sea coupling. The highest improvement is noticed by reducing the wet bias of up to 50–500% caused by SST cooling response due to precipitation that suppresses the convection and hence convective precipitation. Comparatively, a lesser bias reduction is noticed over the Indian land region with a maximum of 50% (30%) over western (eastern) central India. The anomalous warming over AS weakens the zonal SST gradient and hence southwesterly winds, which should substantially diminish the moisture supply towards India (Roxy et al. 2017).

The improvement of precipitation in ROM is a combined effect of improvement in convective and large-scale precipitation (CP and LP). Thus, their contribution to the total improvement of mean precipitation is analyzed. The analysis shows that both contributed to the total improvement. However, these improvements due to CP and LP are region-specific. In general, the improvement over the ocean is mainly associated with suppressed CP due to negative feedback by the inclusion of air–sea coupling. In contrast, both CP and LP contribute to the overall improvement over Indian land regions. The suppressed/enhanced LP/CP over western/eastern central India in the ROM model reduces the REMO's wet/dry bias. Besides, we also observed some regions where air–sea coupling showed minor improvements. For example, the dry (wet) bias over Tibetan Plateau, northern India, and Indo Gangetic plains for CP (precipitation and LP) noticed in REMO also persists in ROM, suggesting an insignificant improvement due to air–sea coupling over these regions. The weakening of moisture-laden low-level Somalia Jet in ROM causes the diminishing of moisture supply from the Arabian Sea towards the Indian land region. The suppressed moisture availability over the region hampers the mean precipitation and reduces wet bias, especially in west central India. The minimal improvement due to air–sea coupling is partially related to persistent SST bias and partially due to the dominant role of atmospheric internal dynamics of the coupled system. Some earlier studies have also highlighted the role of the atmospheric internal dynamics as underlying mechanisms for this propagation (Jiang et al. 2004, 2011; Abhik et al. 2013). We also examined the effects of air–sea coupling on the ISMR relationship with dynamical and thermodynamical indexes using statistical analysis. A similar relationship between indexes and precipitation over India in both models reveals that air–sea coupling does not modulate the relationship of ISMR with dynamical and thermodynamical indexes. The feedback processes due to air–sea coupling alter the strength of indexes and corresponding ISMR in the same direction, unstirring the relationship. Despite a significant improvement in ISM characteristics and associated processes, slight wet bias over western central India persists in ROM. This is partially attributed to the persistence of warm and cold SST bias. A detailed study of the exact mechanism responsible for the persistent wet bias over western central

India in ROM is beyond the scope of this paper, remains a concern for future study.

Supplementary Information The online version contains supplementary material available at https://doi.org/10.1007/s00382-022-06249-6.

Acknowledgements This work is jointly supported by the Department of Science and Technology (DST), Govt. of India, grant number DST/INT/RUS/RSF/P-33/G, and the Russian Science Foundation (Project No.: 19-47-02015). PK acknowledges funding from the Science and Engineering Research Board (SERB), Govt. of India grant number SB/S2/RJN-080/2014, and Department of Science and Technology (DST) grant number DST/CCP/NCM/69/2017(G). The resources of the Deutsches Klimarechenzentrum (DKRZ) granted by its Scientific Steering Committee (WLA) under project ID ba1144 are used to carry out the simulation. The authors are thankful to the respective agencies of the IMD, HadlSST, and ECMWF ERA-Interim data products for making these datasets available. The authors declared that the manuscript contents are novel and neither published nor under consideration anywhere else. The authors also declared that they have no known financial interest.

Declarations

Conflict of interest The authors declared that the contents of the manuscript are novel and neither published nor under consideration anywhere else. The authors also declared that they have no known financial interest.

References

Aadhar S, Mishra V (2020) On the projected decline in droughts over South Asia in CMIP6 multimodel ensemble. J Geophys Res Atmos. https://doi.org/10.1029/2020JD033587

Abhik S, Halder M, Mukhopadhyay P, Jiang Goswami BN (2013) A possible new mechanism for northward propagation of boreal summer intraseasonal oscillations based on TRMM and MERRA reanalysis. Clim Dyn 40(7–8):1611–1624. https://doi.org/10.1007/s00382-012-1425-x

Ashfaq M, Shi Y, Tung WW et al (2009) Suppression of south Asian summer monsoon precipitation in the 21st century. Geophys Res Lett. https://doi.org/10.1029/2008GL036500

Ashfaq M, Rastogi D, Mei R et al (2017) Sources of errors in the simulation of south Asian summer monsoon in the CMIP5 GCMs. Clim Dyn 49:193–223. https://doi.org/10.1007/s00382-016-3337-7

Asselin R (1972) Frequency filter for time integrations. Mon Weather Rev 100:487–490. https://doi.org/10.1175/1520-0493(1972)100%3c0487:fffti%3e2.3.co;2

Beck HE, Wood EF, Pan M et al (2019) MSWep v2 Global 3-hourly 0.1° precipitation: methodology and quantitative assessment. Bull Am Meteorol Soc 100:473–500. https://doi.org/10.1175/BAMS-D-17-0138.1

Cabos W, de la Vara A, Álvarez-García FJ et al (2020) Impact of ocean-atmosphere coupling on regional climate: the Iberian Peninsula case. Clim Dyn 54:4441–4467. https://doi.org/10.1007/s00382-020-05238-x

Cha DH, Jin CS, Moon JH, Lee DK (2016) Improvement of regional climate simulation of East Asian summer monsoon by coupled air–sea interaction and large-scale nudging. Int J Climatol 36:334–345. https://doi.org/10.1002/joc.4349

Charney JG, Shukla J (1981) Predictability of monsoon. In: Lighthill J, Pearce RP (eds) Monsoon dynamics. Cambridge University Press, pp 99–110

Dash SK, Shekhar MS, Singh GP (2006) Simulation of Indian summer monsoon circulation and rainfall using RegCM3. Theor Appl Climatol 86:161–172. https://doi.org/10.1007/s00704-006-0204-1

Davies HC (1976) A lateral boundary formulation for multi-level prediction models. Q J R Meteorol Soc 102:405–418. https://doi.org/10.1002/qj.49710243210

Dee DP, Uppala SM, Simmons AJ et al (2011) The ERA-Interim reanalysis: configuration and performance of the data assimilation system. Q J R Meteorol Soc 137:553–597. https://doi.org/10.1002/qj.828

Di Sante F, Coppola E, Farneti R, Giorgi F (2019) Indian Summer Monsoon as simulated by the regional earth system model RegCM-ES: the role of local air–sea interaction. Clim Dyn 53:759–778. https://doi.org/10.1007/s00382-019-04612-8

Fathrio I, Iizuka S, Manda A et al (2017) Assessment of western Indian Ocean SST bias of CMIP5 models. J Geophys Res Ocean 122:3123–3140. https://doi.org/10.1002/2016JC012443

Giorgi F (2019) Thirty years of regional climate modeling: where are we and where are we going next? J Geophys Res Atmos 124:5696–5723. https://doi.org/10.1029/2018JD030094

Goswami BN, Xavier PK (2005a) ENSO control on the south Asian monsoon through the length of the rainy season. Geophys Res Lett 32:1–4. https://doi.org/10.1029/2005GL023216

Goswami BN, Xavier PK (2005b) Dynamics of "internal" interannual variability of the Indian summer monsoon in a GCM. J Geophys Res Atmos 110:1–17. https://doi.org/10.1029/2005JD006042

Griffies SM (1998) The Gent-McWilliams skew flux. J Phys Oceanogr 28:831–841. https://doi.org/10.1175/1520-0485(1998)028%3c0831:TGMSF%3e2.0.CO;2

Hagemann S, Dümenil L (1998) A parametrization of the lateral waterflow for the global scale. Clim Dyn 14:17–31. https://doi.org/10.1007/s003820050205

Hagemann S, Dumenildumenil L (1998) A parametrization of the lateral waterflow for the global scale. Springer, New York

Hagos SM, Cook KH (2009) Development of a coupled regional model and its application to the study of interactions between the West African monsoon and the Eastern tropical Atlantic Ocean. J Clim 22:2591–2604. https://doi.org/10.1175/2008JCLI2466.1

Hersbach H, Bell B, Berrisford P et al (2020) The ERA5 global reanalysis. Q J R Meteorol Soc 146:1999–2049. https://doi.org/10.1002/qj.3803

Hibler WD (1979) A dynamic thermodynamic sea ice model. J Phys Oceanogr 9:815–846. https://doi.org/10.1175/1520-0485(1979)009%3c0815:ADTSIM%3e2.0.CO;2

Hirons LC, Klingaman NP, Woolnough SJ (2018) The impact of air–sea interactions on the representation of tropical precipitation extremes. J Adv Model Earth Syst 10:550–559. https://doi.org/10.1002/2017MS001252

Jacob D (2001) A note to the simulation of the annual and inter-annual variability of the water budget over the Baltic Sea drainage basin. Meteorol Atmos Phys 77:61–73. https://doi.org/10.1007/s007030170017

Jacob D, Podzun R (1997) Sensitivity studies with the regional climate model REMO. Meteorol Atmos Phys 63:119–129. https://doi.org/10.1007/BF01025368

Jacob D, Elizalde A, Haensler A et al (2012) Assessing the transferability of the regional climate model REMO to different coordinated regional climate downscaling experiment (CORDEX) Regions. Atmosphere (basel) 3:181–199. https://doi.org/10.3390/atmos3010181

Jiang X, Li T, Wang B (2004) Structures and mechanisms of the northward propagating boreal summer intraseasonal oscillation. J Clim

17:1022–1039. https://doi.org/10.1175/1520-0442(2004)017%3c1022:SAMOTN%3e2.0.CO;2
Jiang X, Waliser DE, Li JL, Woods C (2011) Vertical cloud structures of the boreal summer intraseasonal variability based on CloudSat observations and ERA-interim reanalysis. Clim Dyn 36:2219–2232. https://doi.org/10.1007/s00382-010-0853-8
Jungclaus JH, Fischer N, Haak H et al (2013) Characteristics of the ocean simulations in the Max Planck Institute Ocean Model (MPIOM) the ocean component of the MPI-Earth system model. J Adv Model Earth Syst 5:422–446. https://doi.org/10.1002/jame.20023
Kitoh A (2017) The Asian Monsoon and its future change in climate models: a review. J Meteorol Soc Japan Ser II 95:7–33. https://doi.org/10.2151/jmsj.2017-002
Kitoh A, Endo H, Krishna Kumar K et al (2013) Monsoons in a changing world: a regional perspective in a global context. J Geophys Res Atmos 118:3053–3065
Klingaman NP, Woolnough SJ (2014) The role of air–sea coupling in the simulation of the Madden-Julian oscillation in the Hadley Centre model. Q J R Meteorol Soc 140:2272–2286. https://doi.org/10.1002/qj.2295
Konwar M, Parekh A, Goswami BN (2012) Dynamics of east-west asymmetry of Indian summer monsoon rainfall trends in recent decades. Geophys Res Lett. https://doi.org/10.1029/2012GL052018
Kripalani RH, Kulkarni A, Sabade SS (2003) Western Himalayan snow cover and Indian monsoon rainfall: a re-examination with INSAT and NCEP/NCAR data. Theor Appl Climatol 74:1–18. https://doi.org/10.1007/s00704-002-0699-z
Krishnamurti TN (1985) Summer monsoon experiment—a review. Mon Weather Rev 113:1590–1626. https://doi.org/10.1175/1520-0493(1985)113%3c1590:SMER%3e2.0.CO;2
Kumar D, Dimri AP (2020) Context of the added value in coupled atmosphere-land RegCM4–CLM4.5 in the simulation of Indian summer monsoon. Clim Dyn. https://doi.org/10.1007/s00382-020-05481-2
Kumar KK, Rajagopalan B, Hoerling M et al (2006) Unraveling the mystery of Indian monsoon failure during El Niño. Science (80-) 314:115–119. https://doi.org/10.1126/science.1131152
Kumar P, Wiltshire A, Mathison C et al (2013) Downscaled climate change projections with uncertainty assessment over India using a high resolution multi-model approach. Sci Total Environ 468–469:S18–S30. https://doi.org/10.1016/j.scitotenv.2013.01.051
Kumar P, Podzun R, Hagemann S, Jacob D (2014) Impact of modified soil thermal characteristic on the simulated monsoon climate over south Asia. J Earth Syst Sci 123:151–160. https://doi.org/10.1007/s12040-013-0381-0
Kumar D, Rai P, Dimri AP (2020) Investigating Indian summer monsoon in coupled regional land–atmosphere downscaling experiments using RegCM4. Clim Dyn 54:2959–2980. https://doi.org/10.1007/s00382-020-05151-3
Kumar P, Maam VD (2021) CO meeting organizer EGU21. In: Impact of horizontal resolution on indian summer monsoon in coupled atmosphere-ocean regional model over CORDEX-SA
Levine RC, Turner AG (2012) Dependence of Indian monsoon rainfall on moisture fluxes across the Arabian Sea and the impact of coupled model sea surface temperature biases. Clim Dyn 38:2167–2190. https://doi.org/10.1007/s00382-011-1096-z
Li T, Zhou GQ (2010) Preliminary results of a regional air–sea coupled model over East Asia. Chin Sci Bull 55:2295–2305. https://doi.org/10.1007/s11434-010-3071-1
Lucas-Picher P, Christensen JH, Saeed F et al (2011) Can regional climate models represent the Indian monsoon? J Hydrometeorol 12:849–868. https://doi.org/10.1175/2011JHM1327.1
Marsland SJ, Haak H, Jungclaus JH et al (2002) The Max-Planck-Institute global ocean/sea ice model with orthogonal curvilinear coordinates. Ocean Model 5:91–127. https://doi.org/10.1016/S1463-5003(02)00015-X
Marsland SJ, Jungclaus JH, Latif M, Rr Oske F (2003) The Max-Planck-Institute global ocean/sea ice model with orthogonal curvilinear coordinates
Meehl GA, Covey C, Delworth T et al (2007) The WCRP CMIP3 multimodel dataset: a new era in climatic change research. Bull Am Meteorol Soc 88:1383–1394. https://doi.org/10.1175/BAMS-88-9-1383
Mishra AK, Dwivedi S (2019) Assessment of convective parametrization schemes over the Indian subcontinent using a regional climate model. Theor Appl Climatol 137:1747–1764. https://doi.org/10.1007/s00704-018-2679-y
Mishra AK, Dwivedi S, Das S (2020a) Role of Arabian Sea warming on the Indian summer monsoon rainfall in a regional climate model. Int J Climatol 40:2226–2238. https://doi.org/10.1002/joc.6328
Mishra AK, Dwivedi S, Di Sante F, Coppola E (2020b) Thermodynamical properties associated with the Indian summer monsoon rainfall using a regional climate model. Theor Appl Climatol 141:587–599. https://doi.org/10.1007/s00704-020-03237-w
Mishra AK, Dwivedi S, Di Sante F (2021a) Performance of the RegCM-MITgcm coupled regional model in simulating the indian summer monsoon rainfall. Pure Appl Geophys. https://doi.org/10.1007/s00024-020-02648-0
Mishra AK, Kumar P, Dubey AK et al (2021b) Impact of horizontal resolution on monsoon precipitation for CORDEX-South Asia: a regional earth system model assessment. Atmos Res 259:105681. https://doi.org/10.1016/j.atmosres.2021.105681
Misra V, Mishra A, Bhardwaj A (2017) High-resolution regional-coupled ocean–atmosphere simulation of the Indian Summer Monsoon. Int J Climatol 37:717–740. https://doi.org/10.1002/joc.5034
Nagura M, Sasaki W, Tozuka T et al (2013) Longitudinal biases in the Seychelles Dome simulated by 35 ocean–atmosphere coupled general circulation models. J Geophys Res Ocean 118:831–846. https://doi.org/10.1029/2012JC008352
Nagura M, Mccreary JP, Annamalai H (2018) Origins of coupled model biases in the Arabian Sea climatological state. J Clim 31:2005–2029. https://doi.org/10.1175/JCLI-D-17-0417.1
Parth Sarthi P, Ghosh S, Kumar P (2015) Possible future projection of Indian Summer Monsoon Rainfall (ISMR) with the evaluation of model performance in Coupled Model Inter-comparison Project Phase 5 (CMIP5). Glob Planet Change 129:92–106. https://doi.org/10.1016/j.gloplacha.2015.03.005
Parthasarathy (1995) Monthly and seasonal rainfall series for all India, homogeneous regions and meteorological subdivisions: 1871–1994. Res. Rep. No. 65 (Indian Institute of Tropical Meteorology, Pune, India, 1995)
Pathak A, Ghosh S, Kumar P, Murtugudde R (2017) Role of oceanic and terrestrial atmospheric moisture sources in intraseasonal variability of indian summer monsoon rainfall. Sci Rep 7:1–11. https://doi.org/10.1038/s41598-017-13115-7
Pattanaik DR, Rajeevan M (2010) Variability of extreme rainfall events over India during southwest monsoon season. Meteorol Appl 17:88–104. https://doi.org/10.1002/met.164
Rai PK, Singh GP, Dash SK (2020) Projected changes in extreme precipitation events over various subdivisions of India using RegCM4. Clim Dyn 54:247–272. https://doi.org/10.1007/s00382-019-04997-6
Rajeevan M, Bhate J, Jaswal AK (2008) Analysis of variability and trends of extreme rainfall events over India using 104 years of gridded daily rainfall data. Geophys Res Lett. https://doi.org/10.1029/2008GL035143

Raju A, Parekh A, Chowdary JS, Gnanaseelan C (2015) Assessment of the Indian summer monsoon in the WRF regional climate model. Clim Dyn 44:3077–3100. https://doi.org/10.1007/s00382-014-2295-1

Ratnam JV, Giorgi F, Kaginalkar A, Cozzini S (2009) Simulation of the Indian monsoon using the RegCM3-ROMS regional coupled model. Clim Dyn 33:119–139. https://doi.org/10.1007/s00382-008-0433-3

Ratnam JV, Morioka Y, Behera SK, Yamagata T (2015) A model study of regional air–sea interaction in the austral summer precipitation over southern Africa. J Geophys Res 120:2342–2357. https://doi.org/10.1002/2014JD022154

Rechid D, Raddatz TJ, Jacob D (2009) Parameterization of snow-free land surface albedo as a function of vegetation phenology based on MODIS data and applied in climate modelling. Theor Appl Climatol 95:245–255. https://doi.org/10.1007/s00704-008-0003-y

Ren X, Qian Y (2005) A coupled regional air–sea model, its performance and climate drift in simulation on the East Asian summer monsoon in 1998. Int J Climatol 25:679–692. https://doi.org/10.1002/joc.1137

Roeckner E, Bäuml G, Bonaventura L et al (2003) Model description. Max-Planck-Institut für Meteorologie, Hamburg

Roxy MK, Ghosh S, Pathak A et al (2017) A threefold rise in widespread extreme rain events over central India. Nat Commun. https://doi.org/10.1038/s41467-017-00744-9

Sabeerali CT, Ramu Dandi A, Dhakate A et al (2013) Simulation of boreal summer intraseasonal oscillations in the latest CMIP5 coupled GCMs. J Geophys Res Atmos 118:4401–4420. https://doi.org/10.1002/jgrd.50403

Sabeerali CT, Rao SA, Dhakate AR et al (2015) Why ensemble mean projection of south Asian monsoon rainfall by CMIP5 models is not reliable? Clim Dyn 45:161–174. https://doi.org/10.1007/s00382-014-2269-3

Saeed F, Hagemann S, Jacob D (2009) Impact of irrigation on the South Asian summer monsoon. Geophys Res Lett. https://doi.org/10.1029/2009GL040625

Saha A, Ghosh S, Sahana AS, Rao EP (2014) Failure of CMIP5 climate models in simulating post-1950 decreasing trend of Indian monsoon. Geophys Res Lett 41:7323–7330. https://doi.org/10.1002/2014GL061573

Samala BK, Banerjee S et al (2013) Study of the Indian summer monsoon using WRF-ROMS regional coupled model simulations. Atmos Sci Lett 14:20–27. https://doi.org/10.1002/asl2.409

Sayantani O, Gnanaseelan C, Chowdary JS et al (2016) Arabian Sea SST evolution during spring to summer transition period and the associated processes in coupled climate models. Int J Climatol 36:2541–2554. https://doi.org/10.1002/joc.4511

Sein DV, Mikolajewicz U, Gröger M et al (2015) Regionally coupled atmosphere–ocean–sea ice-marine biogeochemistry model ROM: 1. Description and validation. J Adv Model Earth Syst 7:268–304. https://doi.org/10.1002/2014MS000357

Sein DV, Gröger M, Cabos W et al (2020) Regionally Coupled Atmosphere–Ocean-Marine Biogeochemistry Model ROM: 2. Studying the Climate Change Signal in the North Atlantic and Europe. J Adv Model Earth Syst. https://doi.org/10.1029/2019MS001646

Shashikanth K, Salvi K, Ghosh S, Rajendran K (2014) Do CMIP5 simulations of Indian summer monsoon rainfall differ from those of CMIP3? Atmos Sci Lett 15:79–85. https://doi.org/10.1002/asl2.466

Shashikanth et al (2014) Development of a new high spatial resolution (0.25Â° –0.25Â°) long period (1901–2010) daily gridded rainfall data set over India and its comparison with existing data sets over the region

Singh GP, Chattopadhyay J (1998) Relationship of tropospheric temperature anomaly with Indian southwest monsoon rainfall. Int J Climatol 18:759–763. https://doi.org/10.1002/(SICI)1097-0088(19980615)18:7%3c759::AID-JOC288%3e3.0.CO;2-P

Sitz LE, Di Sante F, Farneti R et al (2017) Description and evaluation of the Earth System Regional Climate Model (Reg CM-ES). J Adv Model Earth Syst 9:1863–1886. https://doi.org/10.1002/2017MS000933

Sperber KR, Annamalai H (2008) Coupled model simulations of boreal summer intraseasonal (30–50 day) variability Part 1: Systematic errors and caution on use of metrics. Clim Dyn 31(2–3):345–372. https://doi.org/10.1007/s00382-008-0367-9

Sperber KR, Annamalai H, Kang IS et al (2013) The Asian summer monsoon: an intercomparison of CMIP5 vs. CMIP3 simulations of the late 20th century. Clim Dyn 41:2711–2744. https://doi.org/10.1007/s00382-012-1607-6

Srivastava A, Dwivedi S, Mishra AK (2018) Investigating the role of air–sea forcing on the variability of hydrography, circulation, and mixed layer depth in the Arabian Sea and Bay of Bengal. Oceanologia 60:169–186. https://doi.org/10.1016/j.oceano.2017.10.001

Steele M, Morley R, Ermold W (2001) PHC: a global ocean hydrography with a high-quality Arctic Ocean. J Clim. https://doi.org/10.1175/1520-0442(2001)014%3c2079:PAGOHW%3e2.0.CO;2

Stockhause M, Lautenschlager M (2017) CMIP6 data citation of evolving data. Data Sci J 16:1–13. https://doi.org/10.5334/dsj-2017-030

Stroeve JC, Kattsov V, Barrett A et al (2012) Trends in Arctic sea ice extent from CMIP5, CMIP3 and observations. Geophys Res Lett. https://doi.org/10.1029/2012GL052676

Taylor KE, Stouffer RJ, Meehl GA (2012) An overview of CMIP5 and the experiment design. Bull Am Meteorol Soc 93:485–498

Thomas M, Sündermann J, Maier-Reimer E (2001) Consideration of ocean tides in an OGCM and impacts on subseasonal to decadal polar motion excitation. Geophys Res Lett. https://doi.org/10.1029/2000GL012234

Tiedtke M (1989) A comprehensive mass flux scheme for cumulus parameterization in largescale models. Mon Weather Rev 117:1779–1800

Tompkins A (2002) A prognostic parameterization for the subgrid-scale variability of water vapor and clouds in large-scale models and its use to diagnose cloud cover. J Atmos Sci 59:1917–1942

Valcke S (2013) The OASIS3 coupler: a European climate modelling community software. Geosci Model Dev 6:373–388. https://doi.org/10.5194/gmd-6-373-2013

Webster PJ, Yang S (1992) Monsoon and Enso: selectively interactive systems. Q J R Meteorol Soc 118:877–926. https://doi.org/10.1002/qj.49711850705

Xue P, Malanotte-Rizzoli P, Wei J, Eltahir EAB (2020) Coupled ocean–atmosphere modeling over the maritime continent: a review. J Geophys Res Ocean. https://doi.org/10.1029/2019JC014978

Zhu S, Remedio ARC, Sein DV et al (2020) Added value of the regionally coupled model ROM in the East Asian summer monsoon modeling. Theor Appl Climatol. https://doi.org/10.1007/s00704-020-03093-8

Zou L (2020) Does regional air–sea coupling improve the simulation of the summer monsoon over the western North Pacific in the WRF4 model? Atmos Ocean Sci Lett 13:500–508. https://doi.org/10.1080/16742834.2020.1819755

Zou L, Zhou T (2013) Can a regional ocean–atmosphere coupled model improve the simulation of the interannual variability of the western North Pacific summer monsoon? J Clim 26:2353–2367. https://doi.org/10.1175/JCLI-D-11-00722.1

Zou L, Zhou T (2016) A regional ocean–atmosphere coupled model developed for CORDEX East Asia: assessment of Asian summer monsoon simulation. Clim Dyn 47:3627–3640. https://doi.org/10.1007/s00382-016-3032-8